minerals

MDPI

Article

Recycling of Au during Serpentinization of Ultramafic Rocks: A Case Study from Neoproterozoic Forearc Ophiolites, Egypt

Basem Zoheir [1,*], Astrid Holzheid [2], Aliaa Diab [3], Azza Ragab [4], Fatma Deshesh [4] and Amr Abdelnasser [5,6]

[1] Department of Geosciences, King Fahd University of Petroleum and Minerals, Dhahran 31261, Saudi Arabia
[2] Institute of Geosciences, University of Kiel (CAU), D-24118 Kiel, Germany
[3] Department of Geology, Faculty of Science, Ain Shams University, Cairo 11566, Egypt
[4] Department of Geology, Faculty of Science, Mansoura University, El-Mansoura 35516, Egypt
[5] Department of Geology, Faculty of Science, Benha University, Benha 13518, Egypt
[6] Department of Geological Engineering, Faculty of Mines, Istanbul Technical University, Istanbul 34469, Turkey
* Correspondence: basem.zoheir@gmail.com or basem.zoheir@ifg.uni-kiel.de

Abstract: Gold, along with other highly siderophile elements, is hosted by Fe-Ni sulfide phases within peridotites and mantle melts. In this context, the lithospheric mantle emerges as a principal reservoir, providing materials crucial for the inception, augmentation, conveyance, and genesis of auriferous CO_2-rich mantle fluids. EPMA and laser ablation ICP-MS data, integrated with petrographic and SEM studies, were used to assess the transfer of base and precious metals into the Earth's crust, discerning between inputs from subduction-related processes and post-formation metasomatism. The study focuses on sulfide minerals in serpentinized peridotites of the Abu Dahr ophiolite in the Eastern Desert of Egypt. Originating in a supra-subduction setting during the Neoproterozoic era, the Abu Dahr peridotites underwent serpentinization and contain discrete sulfide minerals, including pentlandite, nickeloan pyrrhotite, millerite, chalcopyrite, and violarite. The uneven distribution of calcite ± magnesite ± serpentine veins throughout the host ophiolitic rocks reflects the intricate interplay of serpentinization and carbonation, as fO_2 and fCO_2 conditions fluctuated. Geochemical data of the host rocks reveal a progressive geochemical evolution marked by concurrent silicification and carbonate alteration, driven by the interaction of ultramafic rocks with hydrothermal fluids, ultimately leading to the extensive silicification and formation of birbirite. The ICP-MS data show that pentlandite contains up to 6.11 ppm of Au, pyrrhotite up to 0.41 ppm, millerite 0.34 ppm, and violarite 0.12 ppm. The gold concentration in pentlandite is significantly higher than in pyrrhotite, millerite, and violarite, which exhibit lower but detectable levels of Au. Desulfurization reactions of sulfide minerals during progressive serpentinization triggered the release and redistribution of Au as well as base metals and highly siderophile elements. Published thermodynamic modeling at temperatures below 300 °C and pressures of 50 MPa closely replicates the mineral assemblage observed in the Abu Dahr ophiolites, including sulfide assemblages and variations in major elements such as Mg and Fe. This suggests that the serpentinization process, along with associated hydrothermal fluids, played a crucial role in the mobilization and redistribution of gold, particularly affecting its incorporation into secondary sulfides. The mobilization of Au and other highly siderophile elements during serpentinization occurred in an environment marked by strong oxidation, as indicated by the presence of acicular antigorite, magnetite, millerite, and goethite intergrowths.

Keywords: mantle sulfides; trace element composition; EPMA; LA-ICP-MS data; serpentinization and Au recycling in subduction zones; Neoproterozoic ophiolites; Egypt

check for updates

Citation: Zoheir, B.; Holzheid, A.; Diab, A.; Ragab, A.; Deshesh, F.; Abdelnasser, A. Recycling of Au during Serpentinization of Ultramafic Rocks: A Case Study from Neoproterozoic Forearc Ophiolites, Egypt. *Minerals* **2024**, *14*, 916. https://doi.org/10.3390/min14090916

Academic Editor: Federica Zaccarini

Received: 5 July 2024
Revised: 2 September 2024
Accepted: 4 September 2024
Published: 6 September 2024

Copyright: © 2024 by the authors. Licensee MDPI, Basel, Switzerland. This article is an open access article distributed under the terms and conditions of the Creative Commons Attribution (CC BY) license (https://creativecommons.org/licenses/by/4.0/).

1. Introduction

1.1. Highly Siderophile Elements in Mantle Rocks

Highly siderophile elements (HSEs), encompassing platinum group elements (PGEs), Re, and Au, play pivotal roles in the geochemical processes within mantle rocks. Mantle-derived magmas and the subcontinental lithospheric mantle (SCLM) serve as crucial reservoirs for these elements, exerting influences on the genesis of globally significant base and precious metal deposits, e.g., Mungall [1] and Griffin et al. [2]. According to Luguet and Reisberg [3], the majority of HSEs in the Earth's upper mantle are primarily found within accessory base-metal sulfides (BMSs) of the Ni-Fe-Cu system. The dynamics of HSE recycling within the SCLM are intricately linked to factors such as partial melting, melt percolation, and the ascent of plume magmas [4].

Gold, categorized as an HSE with thiophile (chalcophile) attributes in geological processes, often exhibits association with sulfides [5,6]. While the average Au content in the Earth's crust stands at 4 ppb, mantle rocks typically host concentrations ranging from 10^{-9} to 10^{-8} ppm [6–8]. Notably, sulfide assemblages showcase significantly elevated gold concentrations, ranging from 10^{-4} to 10^{-2}, compared to their mantle peridotite hosts [9]. Distinct geochemical signatures, as evidenced by studies by Large et al. [10], Morey et al. [11], Cook et al. [12], and Cook et al. [13], underline the spatial relationship between primary sulfides housing trace metals and nearby high-concentration metal deposits. Ophiolites, fragments of oceanic lithosphere composed of mafic-ultramafic rocks, further elucidate the interplay between serpentinization processes, hydrothermal fluid interactions, and the formation of ore minerals [14,15].

In the extensively serpentinized peridotites, primary ore minerals such as pentlandite, often accompanied by pyrrhotite and chalcopyrite, are found as inclusions within Fe-Mg silicate minerals and chromite [16]. These inclusions provide valuable insights into sulfur content and the fugacity of hydrogen and oxygen [17,18]. Sulfides such as pyrrhotite, pentlandite, and chalcopyrite, commonly found in ultramafic rocks, can contain trace amounts of Au that may be released into circulating hydrothermal fluids during serpentinization when these sulfides break down. The solubility and mobility of Au in these fluids are significantly influenced by several key factors, including fluid composition, temperature, and pressure conditions. Fluid composition is critical, as ligands like chlorine, sulfur, and CO_2 can form complexes with Au, enhancing its solubility and facilitating its transport within the fluid [19]. The activity of SiO_2 in the fluid further affects the mineralogy of serpentinization, influencing the breakdown of sulfides and the subsequent release of Au. Temperature and pressure also play vital roles; lower temperatures, particularly those <400 °C, favor the stability of serpentine and sulfide minerals [20]. Additionally, the oxidation state of the fluid is a crucial factor, as it governs the stability of Au within the fluid and its ability to form transportable complexes, ultimately determining how Au is mobilized during serpentinization. This process is further enhanced by the production of hydrogen gas (H_2) and reducing conditions prevailing during serpentinization, which can increase the solubility of Au in the fluids. Consequently, Au can be transported over significant distances and redeposited distally in more concentrated forms [21,22].

Serpentinized peridotites commonly preserve high-sulfur mineral assemblages, along with magnetite or hematite, formed during serpentinization. The most significant ore minerals associated with these sulfide assemblages, which represent low-temperature alteration products, include awaruite (Ni_3Fe), wairauite (CoFe), and various base-metal alloys. These minerals reflect the complex alteration processes and chemical interactions occurring within the serpentinized ultramafic rocks [21,23–25]. The formation of Cu-bearing sulfide minerals can occur through two distinct processes: desulfurization of primary sulfides under strongly reducing and sulfur-depleted conditions due to serpentinization, and subsequent interaction with Cu-bearing high-temperature solutions [26]. While Cu-rich sulfides are associated with hydrothermal leaching in mafic sequences, native Cu may result from the alteration of original Cu-bearing sulfide minerals or potentially have a primary origin from the Earth's mantle [27,28].

Gold mobilization during serpentinization and carbonatization of oceanic lithosphere occurs at moderate temperatures (150–250 °C) through the reaction with heterogeneous H_2O–CO_2–CH_4 hydrothermal fluids [29,30].

1.2. Sulfide Inclusions in Ophiolitic Peridotites: Primary vs. Hydrothermal Origins

Sulfide phases, observed in mantle xenoliths and the mantle section of ophiolite complexes, are typically present in concentrations of less than 0.1 wt.% and include pentlandite, pyrrhotite, chalcopyrite, and monosulfide solid solution (MSS), which includes phases such as pyrrhotite and pentlandite, and rare intermediate solid solution (ISS) phases, i.e., cubanite [31]. In these sulfides, Fe is the primary component alongside lesser concentrations of Ni and Cu. According to Guo et al. [32], variations in the composition of mantle sulfides are evident across different rock types. In the peridotite xenoliths, sulfides typically contain around 20 wt.% Ni and 4–5 wt.% Cu. Sulfide abundance controls the behavior of siderophiles, chalcophiles, and PGEs, providing insights into processes such as partial melting and melt migration within the mantle [33–35].

Mantle sulfides can be classified as interstitial (i-type), inclusions within rock-forming minerals (e-type), or minor sulfide phases in metasomatic veinlets and/or silicate-carbonate-interstitial patches (m-type) [36]. The formation of these sulfides involves processes such as re-equilibration of sulfide melts at low temperatures (<300 °C) for i-type sulfides and percolating sulfide–carbonate–silicate fluids or melts during low-temperature metasomatism for the m-type sulfides [36].

Trace element enrichment in sulfides is influenced by physico-chemical factors such as pressure, temperature, oxygen fugacity (fO_2), and the composition of surrounding peridotite [36]. Many of the base metals like Cu, Pb, and Zn, as well as other less common metals such as Ag, As, Au, Bi, Cd, Co, Ga, Ge, In, Hg, Mo, Ni, Re, Sb, Se, Sn, etc., are commonly confined to secondary hydrothermal sulfides. The latter form from hydrothermal fluids, which can stem from magmatic, hydrothermal, or meteoric sources, at temperatures ranging from 500 to 100 °C. Fontboté et al. [37] suggested that the concentration of these metals can be modified by supergene processes of hypogene sulfides, resulting in either an increase or decrease. Throughout these processes, some metals may undergo remobilization and then precipitate in enriched or oxidation zones, while others may become diluted due to their adverse environmental impacts.

The present study investigates the trace element composition of sulfide minerals from Gabal Abu-Dahr serpentinized ophiolitic peridotites using LA-ICP-MS. Our aim is to understand the metal flux during subduction-related processes and metasomatism. Particularly intriguing is the role of serpentinization in Au recycling within subduction zones. Moreover, this study holds promise in significantly expanding our comprehension of geological processes operative in subduction zones, particularly the mobility and concentration of important metals like Au. Such insights may extend beyond the realms of geological research, potentially impacting domains such as mineral exploration and mining.

2. The Gabal Abu Dahr Ophiolite

The Gabal Abu Dahr area, in the South Eastern Desert of Egypt, lies ~70 km northwest of Shalateen on the Red Sea, between latitudes 23°30′ N and 23°40′ N, and longitudes 35°00′ E and 35°08′ E (Figure 1). This area is characterized by four primary tectonic units: autochthonous basal granodiorite gneisses, allochthonous ophiolitic nappes, island-arc volcanic/plutonic rocks, and syn- to late-tectonic granites [38–41]. A tectonic matrix composed of carbonaceous metasediments and metavolcanic rocks contains fragments from pre-existing country rocks (Figure 1).

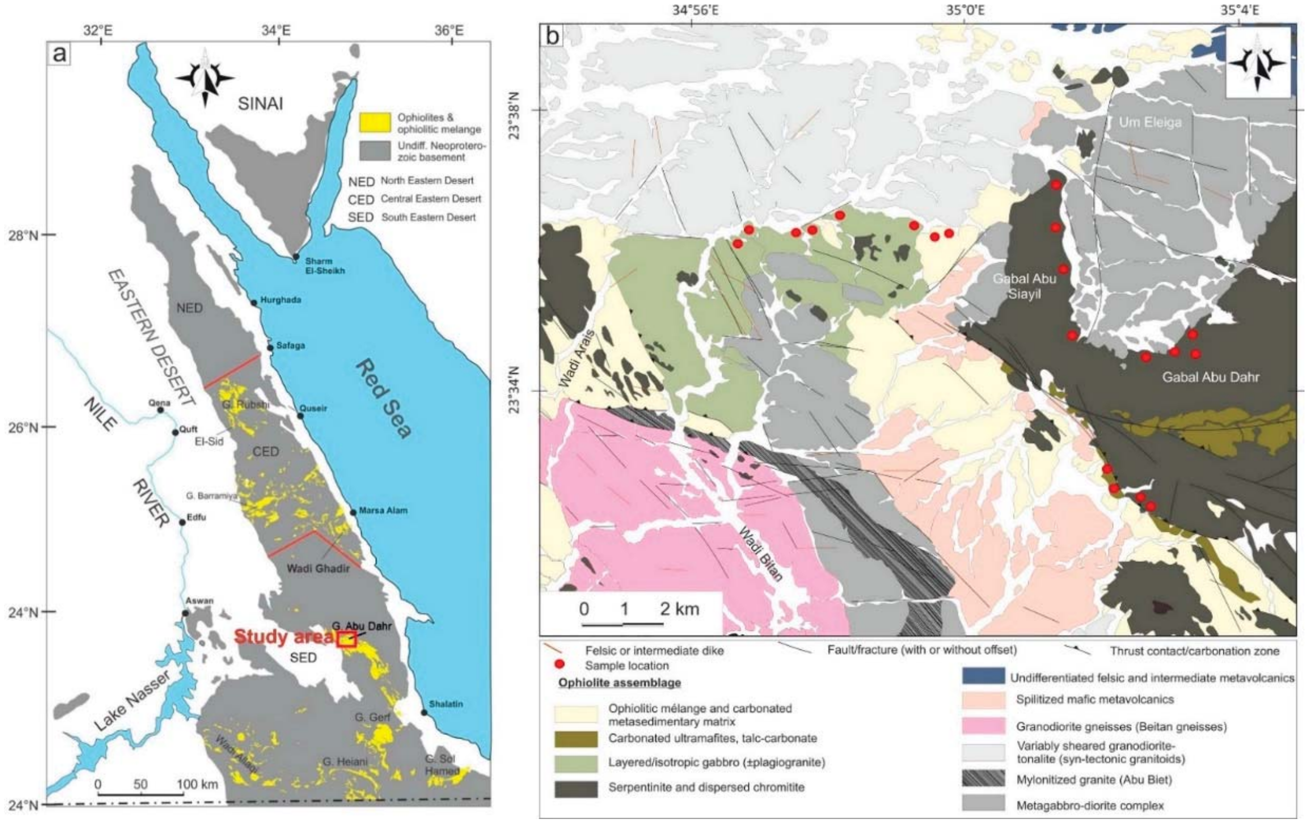

Figure 1. (**a**) Distribution of the ophiolitic block and mélanges in the Eastern Desert of Egypt. Red lines are anticipated tectonic boundaries between different terranes in the Eastern Desert. (**b**) Geologic map of the Gabal Abu Dahr area, adapted from Zoheir et al. [42].

The Gabal Abu Dahr ophiolites encompass fragmented ophiolitic sequences that can attain a maximum thickness of approximately 17 km, as inferred from the cumulative thickness of the exposed mantle and crustal rocks in relevant maps [38–41]. The ophiolitic section comprises serpentinized ultramafic rocks at the lower part, transitioning upward to layered and isotropic gabbroic rocks, followed by sheeted dykes and capped by pillow basalt in the uppermost part [38–41]. The matrix of the mélange predominantly comprises intensely sheared serpentinites and metasedimentary rocks. It also encompasses fragments of metaultramafic rocks, which locally contain chromitite, as well as metagabbro and metabasalt (Figure 1). The metaultramafic rocks are particularly prominent in the Um Eleiga area, manifesting as substantial blocks of serpentinites, including talc-carbonate and listvenite. These lithological units are distributed across Gabal Abu Dahr, Gabal Arias, Gabal Siayil, Gabal Belamhandeit, and Gabal Umm Thagar (Figures 1 and 2a). Discrete chromitite pods were observed within the serpentinites (Figure 2b). The serpentinites of Gabal Abu Dahr host occurrences of listvenite and silicified ultramafic rocks, specifically birbirite.

Petrographically, the serpentinites are predominantly composed of antigorite, chrysotile, lizardite, and bastite, alongside accessory chromite (Figure 2c). The metagabbro units form hills of moderate elevation and contain pockets of pegmatitic and isotropic gabbro. Their mineralogical composition typically includes altered plagioclase, pyroxenes (augite and hypersthene), tremolite, and actinolite, along with secondary alteration minerals such as zoisite, kaolinite, and iron oxides (Figure 2d).

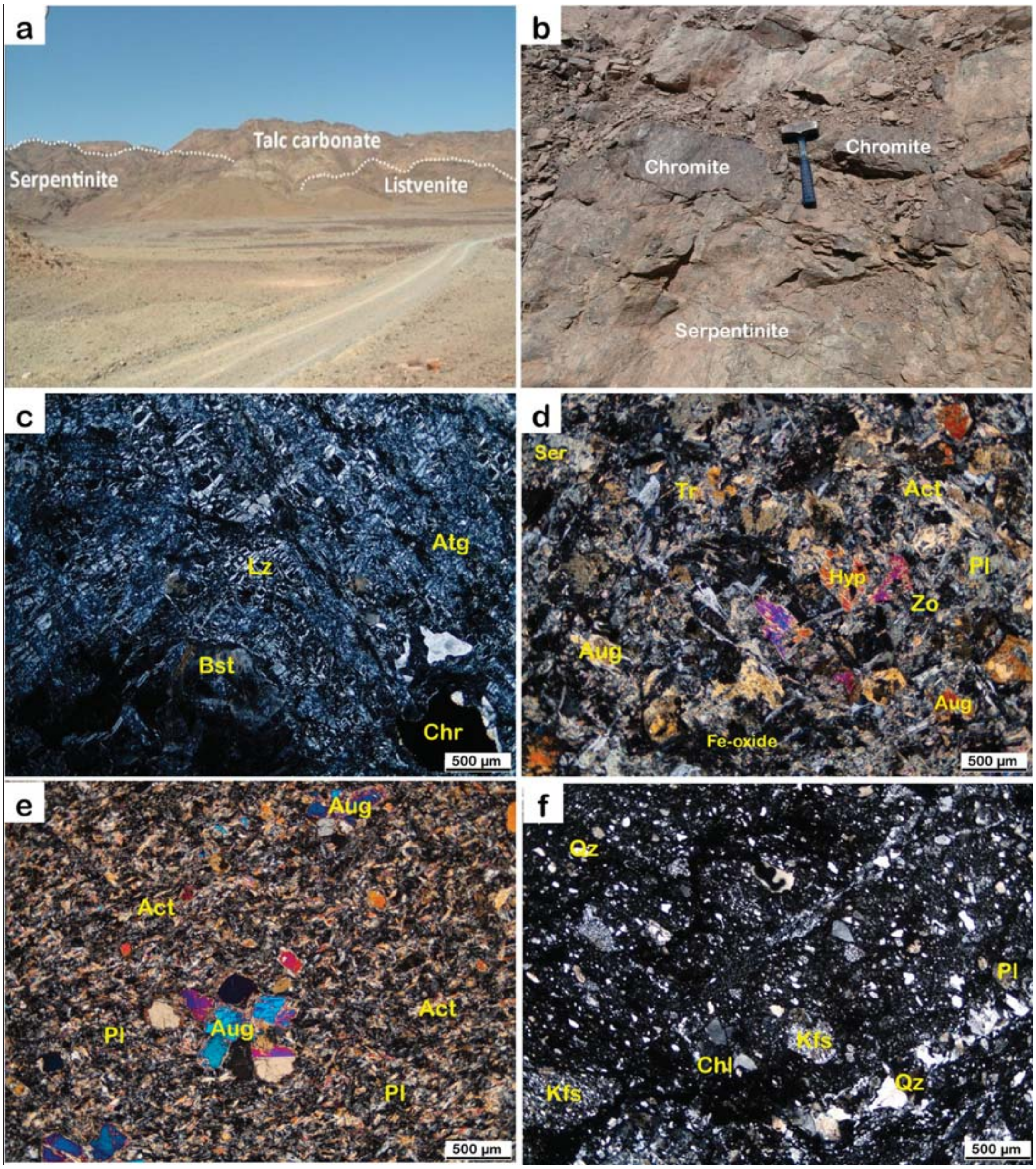

Figure 2. Geological features within the Gabal Abu Dahr area: (**a**) serpentinite with talc-carbonate and listvenite formations at the Um Eleiga area, and (**b**) chromite ore occurrences in serpentinite. Transmitted light (TL) microscope images of the different rock units of the Gabal Abu Dahr area: (**c**) antigorite, lizardite, bastite and chromite in serpentinite (TL), (**d**) metagabbro exhibiting altered plagioclase, pyroxene (augite and hypersthene), tremolite, and actinolite, accompanied by zoisite, sericite, kaolinite, and Fe-oxides (TL), (**e**) pillow metabasalt displaying augite porphyroblasts in a fine-grained matrix of altered plagioclase and actinolite, interspersed with opaque minerals (TL), and (**f**) acidic metatuffs primarily composed of kaolinitized microperthite, chlorite, and quartz, with minor quantities of plagioclase and iron oxide. These are embedded within a much finer tuffaceous matrix consisting of microcrystalline aggregates of kaolinitized feldspar, quartz, and dusty iron oxide (TL). Abbreviations used: actinolite (act), antigorite (ant), augite (aug), bastite (bst), chlorite (chl), chromite (chr), hypersthene (hyp), K-feldspar (kfs), lizardite (Lz), plagioclase (pl), quartz (qz), sericite (ser), tremolite (tr), and zoisite (zo).

In the Gabal Abu Dahr area, metabasalt, distinguished by locally pillowed structures, overlies metagabbro. The metabasalt unit displays a porphyritic texture, characterized by augite porphyroblasts set within a fine-grained matrix of altered plagioclase and actinolite, along with interspersed opaque minerals (Figure 2e). These basal rocks are overlain by volcano-sedimentary formations, predominantly found in the western and northern parts of the study area (Figure 1). Prominent among these formations are acidic metatuffs, primarily composed of kaolinitized microperthite, chlorite, and quartz, with minor plagioclase and iron oxide content. The fine-grained tuffaceous matrix is comprised of kaolinitized feldspar, quartz, and disseminated iron oxide, indicating a complex history of metamorphic alteration and sedimentary deposition within the region (Figure 2f).

3. Field Work and Methods

Fieldwork was carried out in the Gabal Abu Dahr area to gain a comprehensive understanding of the geological context. Samples were systematically collected from both fresh ophiolitic rocks and altered rocks containing sulfide minerals to ensure representativeness. Forty polished sections were obtained from the collected samples and were then petrographically examined using a polarizing microscope to elucidate the mineralogical and textural relationships.

Whole-rock major element analyses of 9 samples (serpentinite and associated rocks) were performed by X-ray fluorescence (XRF) at GEOMAR (Kiel) on fused beads using a Philips X'Unique PW 1480, calibrated with international standards.

Determination of the chemical composition of disseminated sulfide minerals in the investigated samples was carried out using a JEOL JXA-8900R electron probe microanalyzer (JEOL Ltd., Tokyo, Japan), equipped with five wavelength-dispersive spectrometers at the University of Kiel. Operating conditions included an accelerating voltage of 20 kV, a beam current of 30 nA, a spot size of 1 μm, and a measurement period of 10–30 s. External calibration was performed utilizing natural and manufactured silicate standards, and data correction employed the PRZ method (modified ZAF) for all elements.

Trace elements in sulfide minerals were analyzed employing an AGILENT 7900s ICP-MS (Agilent Technologies, Santa Clara, CA, USA), at the University of Kiel, complemented by a Coherent GeoLas Pro HD laser ablation system. To facilitate precision, samples were housed within a Zurich-type low-dispersion high-capacity laser ablation cell (LDHCLAC), supplied with a carrier gas of 1.0 L min^{-1} He. Analyses were conducted by laser-ablating spot sizes ranging from 16 to 32 μm, contingent upon grain size, at a pulse frequency of 5 Hz. The laser beam energy remained consistently set at 2.6 J cm^{-2}. Each sample underwent an analysis period of 90 s, comprising 30 s of background measurement with the laser deactivated and 60 s of active analysis. Measuring parameters were standardized, with a set acquisition time of 0.02 s for all masses, resulting in a total sweep time of 0.6 s.

Data reduction was carried out utilizing the GLITTER 4.5 software program, as proposed by Longerich et al. [43]. This involved employing the graphical visualization tool within GLITTER to define integration intervals for each spot analyzed. External standardization was facilitated through the utilization of standard MASS-1 and FeS-1 nanoparticulate-pressed pellets, as advocated by Garbe-Schönberg and Müller [44]. Additionally, NIST SRM612 silicate glass served as internal standards for GLITTER computations. The concentration of the internal standard element, typically aligned with a major element, within the analyzed spots, was derived through EMPA, leveraging ^{57}Fe concentrations of the materials under scrutiny.

4. Alteration and Sulfide Mineralogy

The alteration of ultramafic rocks in the Gabal Abu Dahr area exhibits a complex history of multiple metamorphic and hydrothermal processes [40,45–47]. The presence of antigorite, lizardite, and bastite in serpentinites indicates extensive serpentinization, where primary minerals such as olivine and pyroxenes were hydrated and converted into serpentine minerals (Figure 3). The occurrence of talc-carbonate and listvenite formations suggests significant carbonation and silicification, processes driven by the influx of CO_2- and silica-rich fluids, leading to the formation of carbonates like talc and magnesite, and quartz, respectively. The identification of chlorite points to chloritization, where serpentine and other minerals were altered under low- to medium-grade metamorphic conditions [40,45–47]. Oxidation processes are evident from the presence of iron oxides, likely formed from the oxidation of sulfide minerals such as pyrite, indicative of later exposure to oxidizing conditions. Furthermore, secondary alterations, including kaolinitization, zoisitization, and sericitization, suggest additional hydrothermal or weathering processes that have affected feldspar-rich rocks.

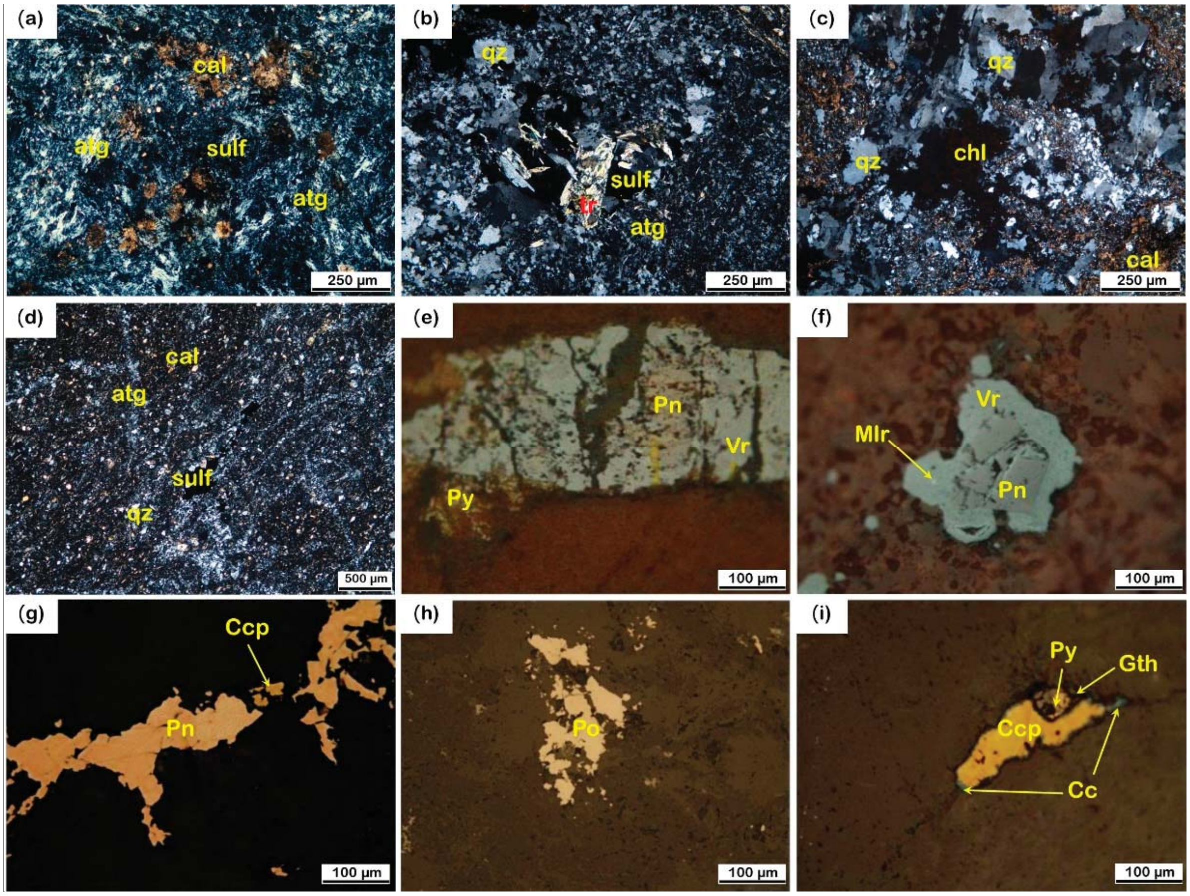

Figure 3. Transmitted (TL) and reflected light (RL) microscope images of the alteration features and base-metal sulfides (BMS) in the Gabal Abu Dahr area: (**a**) sulfide (sulf) associated with antigorite and calcite in carbonatized serpentinite (TL), (**b**) tremolite, antigorite, talc (red marks) and quartz associated with sulfide in silicified serpentinite (TL), (**c**) antigorite, chlorite, calcite, and quartz, the main components of chloritized serpentinite (TL), (**d**) network of quartz veinlets with antigorite and tremolite and disseminated sulfides in birbirite (TL), (**e**) violarite replacing pentlandite with pyrite (RL), (**f**) millerite replacing pentlandite within serpentinized ultramafic rocks (RL), (**g**) disseminated chalcopyrite associated with pentlandite (RL), (**h**) irregular brownish pyrrhotite (RL), and (**i**) rim alteration of chalcopyrite into chalcocite (RL). Abbreviations: antigorite (atg); calcite (cal); chalcocite (Cc); chalcopyrite (Ccp); chlorite (chl); goethite (Gth); millerite (Mlr); pentlandite (Pn); pyrrhotite (Po); pyrite (Py), quartz (qz); sulfide (sulf); and violarite (Vr).

The investigated ophiolitic rocks underwent variable alterations in their mineral composition along thrust faults and shear zones, accompanied by intense deformation. In the Gabal Abu Dahr area, the mineralogical studies reveal that the main alteration products in the serpentinite rocks are silica-carbonate, carbonatized-, silicified-, and chloritized-serpentinite, and birbirite (Figures 3a–d and 4). The birbirite also exhibits distinct features, including a green color, a mesh-like structure with scattered sulfides, and being mostly composed of quartz (85 vol.%) (Figure 3d). Quartz occurs mostly in the form of stockworks and/or subhedral grains. Other components include antigorite and tremolite, accompanied by a significant presence of scattered sulfides (Figure 3d). The sulfide mineralogy of the studied lithologies—serpentinized peridotite, serpentinite, listvenite, and birbirite—exhibits a diverse suite of sulfide minerals with varying degrees of alteration. The main sulfides identified through petrographic and mineralogical investigations (Figure 3e–i) include pentlandite, pyrrhotite, chalcopyrite, pyrite, chalcocite, millerite, violarite, and rare cubanite.

In serpentinized peridotites and serpentinites, pentlandite is a prominent sulfide, occurring as pinkish, euhedral to subhedral crystals that are partially altered to violarite (Figure 3e,f). Pyrrhotite appears as irregular, brownish grains, often associated with pentlandite, while chalcopyrite is found as scattered, irregular grains in association with pentlandite and pyrite, with partial replacement by chalcocite (Figure 3i). Pyrite is also present and is commonly altered to goethite, which occurs as a secondary mineral in the alteration zones (Figure 3i). Millerite forms acicular grains as a replacement of pentlandite, and violarite typically occurs as an irregular replacement of pentlandite.

In listvenite, pyrite is abundant and often alters to goethite, with chalcopyrite appearing as scattered grains. Pentlandite is less common in listvenite and is almost completely altered. In birbirite, pyrite occurs as scattered grains, chalcopyrite as patchy, irregular grains, and millerite is present as dispersed acicular grains. Violarite forms small grains scattered within the serpentine and talc zones, reflecting the complex alteration and mineral replacement processes within these lithologies.

5. Results

5.1. Geochemical Characteristics of Abu Dahr Serpentinites and Alteration Products

The geochemical analysis of the variably altered ophiolitic rocks from the Gabal Abu Dahr area (Table 1), particularly focusing on serpentinite and its alteration products such as listvenite and birbirite, provides important insights into the geological processes that have influenced these rocks. The serpentinite samples exhibit high MgO content, ranging from 37.48% to 41.30%, suggesting that the parent rock, likely peridotite, underwent extensive serpentinization. During this process, primary minerals such as olivine and pyroxene were altered to serpentine minerals [48]. The studied rocks also exhibit variable contents of SiO_2 (36.05% to 41.07%) and consistently low Al_2O_3 (0.81% to 1.42%). The total iron oxide content ($Fe_2O_3{}^t$) ranges from 6.60% to 8.03%, which is consistent with the formation of secondary magnetite during serpentinization. The Loss on Ignition (LOI) values are relatively high, between 10.53% and 14.97%, reflecting the hydrous nature of serpentine minerals [49].

The alteration products, namely listvenite and birbirite, exhibit distinct geochemical signatures that differentiate them from the serpentinite precursor. The listvenite samples show increased SiO_2 contents (43.03% to 44.46%) alongside MgO contents (33.97% to 35.05%), suggesting that significant silica and carbonate minerals were introduced during their formation, likely through hydrothermal processes [50]. The $Fe_2O_3{}^t$ content in listvenite is slightly elevated (8.53% to 8.97%) relative to serpentinite, indicating the involvement of Fe-bearing fluids during the alteration process. The lower LOI values in listvenite (8.02% to 9.02%) compared to serpentinite are indicative of relative dehydration, consistent with the replacement of serpentine by anhydrous carbonate and silica minerals. Conversely, birbirite displays even higher SiO_2 content (49.15% to 50.92%) and a significant reduction in MgO (20.01% to 22.80%), indicating extensive silicification. The observed increase in CaO content (6.85% to 7.14%) and $Fe_2O_3{}^t$ (10.23% to 10.45%) suggests that hydrothermal fluids enriched in calcium and iron contributed to the alteration, leading to the formation of iron-carbonate minerals such as ankerite. This geochemical progression from serpentinite to birbirite highlights a transition toward more silica-rich and carbonate-rich compositions, representing advanced stages of alteration [51].

Table 1. Bulk-rock geochemical data of variably altered ophiolitic rocks from the G. Abu Dahr area.

Rock Type	**Serpentinite**					**Birbirite**		**Listvenite**	
Sample ID	**AD_SP1**	**AD_SP2**	**AD_S1**	**AD_S2**	**AD_S3**	**AD_B1**	**AD_B2**	**AD_L1**	**AD_L2**
SiO_2	41.07	40.48	36.05	37.55	36.82	50.92	49.15	43.03	44.46
TiO_2	0.05	0.08	0.03	0.02	0.03	0.05	0.06	0.07	0.08
Al_2O_3	1.21	1.42	0.81	0.90	0.85	0.15	0.18	1.51	1.61
$Fe_2O_3{}^t$	8.03	7.55	7.48	6.99	6.60	10.23	10.45	8.97	8.53
MnO	0.15	0.10	0.07	0.08	0.07	0.07	0.09	0.10	0.12
MgO	38.99	37.48	40.05	39.04	41.30	20.01	22.80	35.05	33.97
CaO	0.61	0.79	0.15	0.10	0.18	7.14	6.85	0.79	0.85
Na_2O	0.05	0.08	0.02	0.01	0.03	0.02	0.01	0.05	0.06
K_2O	0.02	0.03	0.03	0.02	0.01	0.01	0.02	0.01	0.03
P_2O_5	0.03	0.02	0.01	0.02	0.01	0.01	0.02	0.02	0.03
Cr_2O_3	0.32	0.45	0.21	0.24	0.23	0.31	0.34	0.51	0.55
NiO	0.25	0.35	0.20	0.15	0.22	0.08	0.10	0.20	0.25
LOI	11.05	10.53	13.97	14.97	14.21	10.53	9.05	8.02	9.02
Total	101.83	99.36	99.08	100.09	100.56	99.53	99.12	98.33	99.56

Ternary diagrams further elucidate the geochemical evolution of these rocks. In the SiO_2-Fe_2O_3-CaO + MgO diagram, serpentinite samples cluster toward the MgO-CaO corner, reflecting their ultramafic origin, whereas listvenite and birbirite samples plot closer to the SiO_2 corner, indicating silica enrichment during alteration (Figure 4a). The LOI-SiO_2-CaO + MgO diagram shows a similar trend, with listvenite and birbirite exhibiting lower LOI values, indicative of dehydration during the formation of carbonate and silica minerals (Figure 4b).

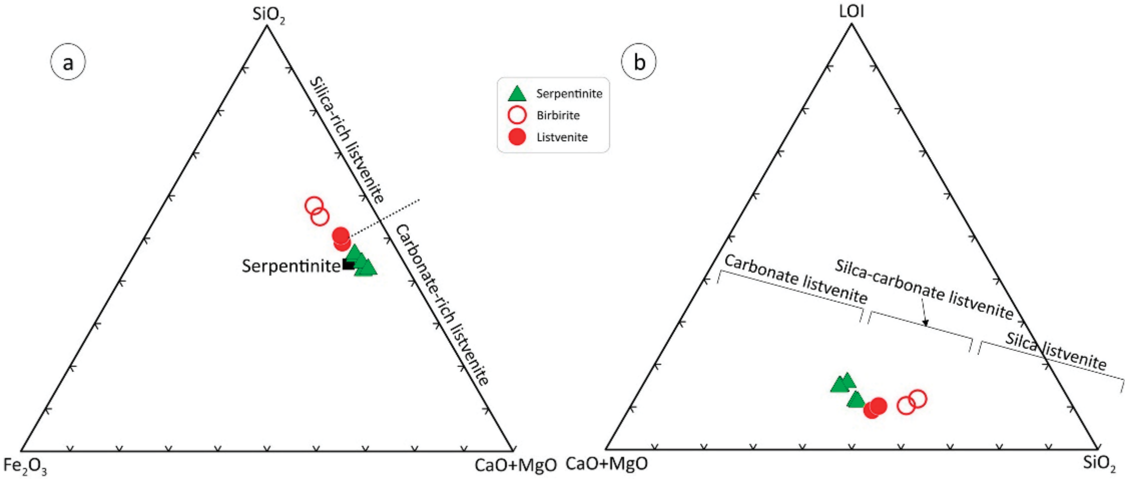

Figure 4. Bulk geochemical variations for serpentinite, listvenite, and birbirite in the G. Abu Dahr area. (**a**) Fe_2O_3-SiO_2-(MgO + CaO) ternary diagram after Akbulut et al. [52]. (**b**) (MgO + CaO)-SiO_2-LOI ternary diagram after Boskabadi et al. [50].

5.2. EMPA Data of Sulfides

The chemical composition of sulfide minerals in the Gabal Abu Dahr ophiolites is given in Table 2 and represented in Figure 5. Sulfides in the ophiolitic units comprise pentlandite, pyrrhotite, chalcopyrite, violarite, and millerite. The results reveal a spectrum of S, Fe, and Ni contents, ranging from 32.25–33.73 wt.%, 26.44–27.38 wt.%, and 36.66–39.28 wt.%, respectively. Remarkably, the stoichiometric composition of pentlandite resembles that of peridotite sulfide, characterized by notably low Co concentrations < 1.71 wt.%. Pyrrhotite, occurring in sub-micrometric intergrowths with other sulfides, exhibits a substantial Ni concentration (up to 10.48 wt.%) alongside notable S and Fe contents, underscoring its classification as Ni-pyrrhotite. Chalcopyrite, the second most prevalent BMS in the examined samples, showcases varying Cu concentrations (33.74–34.67 wt.%) alongside Fe and S concentrations ranging from 29.13–30.41 wt.% and 34.42–35.39 wt.%, respectively. Millerite, commonly associated with pentlandite, demonstrates sulfur content ranging from 30.27–36.05 wt.% and Ni content from 62.70–68.90 wt.%, complemented by traces of Co and As. Violarite is a secondary mineral that develops from the oxidation of primary sulfides like pentlandite and pyrrhotite in the oxidized and weathered zones of the supergene environment, driven by groundwater flow [53]. This transformation often involves intermediate stages, such as the formation of millerite, before pentlandite fully converts to violarite [53]. It manifests varying Fe, Ni, and S contents, with detectable traces of As, delineating its structural formula as $Fe_{1.12}Ni_{2.08}As_{0.01}S_{3.79}$. The intergrowth of magnetite with pyrrhotite and pentlandite is widespread, indicating various forms of intergrowths and aggregates (Figure 5). The high Fe content in Ni-pyrrhotite may indicate a genetic association with magmatic sulfides, formed under high-temperature conditions. Violarite's composition, characterized by high Ni and S, suggests a genetic link to magmatic sulfides.

5.3. Trace Elements of Sulfide Minerals by LA-ICP-MS

LA-ICP-MS spot analyses conducted on suitable-size pentlandite, nickeloan pyrrhotite, chalcopyrite, millerite, and violarite grains from the Gabal Abu Dahr area are detailed in Table 3 and Figures 6 and 7. The measured trace elements encompass siderophile and chalcophile elements, alongside a few lithophile elements. Siderophile elements such as Ni, Co, Mn, Mo, Au, Pd, and Pt and chalcophile elements like Cu, Zn, Cd, Ag, Sn, Pb, Bi, Tl, Sb, Se, and As possess intermediate electro-negativities, which predispose them to form covalent or metallic bonds, respectively [54]. Despite their prevalence in mantle sulfides and sulfide deposits, these elements are comparatively scarce in the Earth's crust relative to their solar abundance. The trace element analysis of disseminated sulfides, including pentlandite, nickeloan pyrrhotite, millerite, and violarite, in the Gabal Abu Dahr serpentinite reveals notable disparities in siderophile element concentrations. Specifically, pentlandite, Ni-pyrrhotite, and millerite exhibit higher concentrations of ^{197}Au and siderophile elements like PGE (e.g., ^{195}Pt, ^{105}Pd, and ^{193}Ir) compared to violarite (Figures 6 and 7). Pentlandite contains higher amounts of ^{197}Au (up to 6.1 ppm) along with other PGEs, while Ni-pyrrhotite and millerite also demonstrate notable concentrations of these elements. Conversely, violarite generally shows lower concentrations of these elements, with ^{197}Au being detected at levels up to 0.12 ppm and the other PGEs present in amounts too small to be reliably measured. Figure 6 demonstrates that earlier magmatic events incorporated significant concentrations of Au and Co into the pentlandite. As serpentinization advances, primary minerals like olivine undergo breakdown, facilitating the mobilization of elements like Au, Co, and Se by hydrothermal fluids. This mobilization results in Au and Co being redistributed into both primary and secondary sulfide minerals, including millerite and violarite, which have been formed by oxidation and alteration of pentlandite. The distribution of Au across minerals like pentlandite and millerite underscores the critical role of serpentinization in concentrating these economically valuable elements within the lithospheric mantle. Additionally, the observed variability in Se concentrations in secondary minerals such as violarite suggests that serpentinization not only alters the mineralogical composition but also influences the re-concentration of these elements under varying geochemical conditions [48,55–58].

Table 2. EPM data of the sulfide inclusions in serpentinized peridotites from the Abu Dahr ophiolites.

Pentlandite: n = 14				**Nickeloan Pyrrhotite: n = 12**				**Chalcopyrite: n = 10**				**Millerite: n = 8**				**Violarite: n = 11**			
wt.%	**Min.**	**Max.**	**Average**	**wt.%**	**Min.**	**Max.**	**Average**	**wt.%**	**Min.**	**Max.**	**Average**	**wt.%**	**Min.**	**Max.**	**Average**	**wt.%**	**Min.**	**Max.**	**Average**
Fe	27.35	28.33	27.99	Fe	53.51	60.92	55.67	Fe	29.13	30.41	30.08	Fe	0.11	0.17	0.14	Fe	13.48	31.10	19.90
S	32.25	33.73	33.17	S	34.66	39.11	36.29	S	34.42	35.39	35.03	S	32.69	36.05	33.96	S	36.97	41.74	38.55
As	0.07	0.13	0.11	As	0.00	0.50	0.06	Ni	0.00	0.06	0.01	As	0.11	0.33	0.19	As	0.00	0.56	0.17
Co	0.00	0.32	0.17	Co	0.00	0.47	0.19	Cu	33.74	34.67	34.35	Co	0.04	0.34	0.19	Ni	24.85	44.38	38.61
Ni	36.66	39.28	37.16	Ni	0.44	10.48	7.30	Sum	97.35	100.15	99.47	Ni	62.70	66.51	64.08	Te	0.11	0.25	0.20
Zn	0.00	0.05	0.03	Sum	97.83	100.43	99.50		atom %			Te	0.29	0.35	0.33	Pb	0.04	0.18	0.11
Sum	97.51	99.88	98.62		atom %			Fe	24.45	25.03	24.80	Sum	97.26	100.42	98.89	Sum	96.08	98.22	97.54
	atom %			Fe	42.63	47.08	44.15	S	50.10	50.66	50.30		atom %				atom %		
Fe	22.58	23.20	23.06	S	48.81	52.78	50.14	Ni	0.00	0.05	0.01	Fe	0.09	0.14	0.12	Fe	11.05	24.36	16.00
S	46.38	47.90	47.60	As	0.00	0.30	0.03	Cu	24.78	25.00	24.89	S	47.21	50.71	49.00	S	52.39	56.94	54.13
As	0.04	0.08	0.07	Co	0.00	0.35	0.14	Sum	100	100	100	As	0.07	0.21	0.12	As	0.00	0.34	0.10
Co	0.00	0.25	0.13	Ni	0.33	7.91	5.54	formula	$Fe_{0.99}Cu_{1.0}S_{2.01}$			Co	0.03	0.27	0.15	Ni	18.51	34.20	29.67
Ni	28.85	30.85	29.13	Sum	100	100	100	Fe	0.98	1.00	0.99	Ni	48.91	52.45	50.50	Te	0.04	0.09	0.07
Zn	0.00	0.04	0.02	formula	$Fe_{0.88}Ni_{0.11}S_{1.00}$			S	2.00	2.03	2.01	Te	0.11	0.13	0.12	Pb	0.01	0.04	0.02
Sum	100	100	100	Fe	0.85	0.94	0.88	Cu	0.99	1.00	1.00	Sum	100	100	100	Sum	100	100	100
formula	$Fe_{3.92}Ni_{4.95}Co_{0.02}As_{0.01}S_{8.09}$			S	0.98	1.06	1.00	Sum	4	4	4	formula	$Ni_{1.01}S_{0.98}$			formula	$Fe_{1.12}Ni_{2.08}As_{0.01}S_{3.79}$		
Fe	3.84	3.94	3.92	Ni	0.01	0.16	0.11					S	0.94	1.01	0.98	Fe	0.77	1.70	1.12
S	7.89	8.14	8.09	Sum	2	2	2					Ni	0.98	1.05	1.01	S	3.67	3.99	3.79
As	0.01	0.01	0.01									Sum	2	2	2	As	0.00	0.02	0.01
Co	0.00	0.04	0.02													Ni	1.30	2.39	2.08
Ni	4.90	5.24	4.95													Sum	7	7	7
Sum	17	17	17																

The correlation between Au and various siderophile elements provides valuable insights into the mechanisms driving the redistribution and concentration of Au during serpentinization processes (Figure 7). Pentlandite, which originated during earlier magmatic events, has a significant positive relationship with Au and Co, indicating their simultaneous incorporation during the crystallization process (Figure 8a,b). Pentlandite serves as the main conduit for Au. This aligns with the role of magmatic sulfides in the concentration of gold, which is then redistributed during hydrothermal processes [59,60]. During the process of serpentinization, pyrrhotite forms from an MSS, exhibiting different relationships between Au and other siderophile elements. In particular, we observe a positive correlation with Mn (Figure 8c), suggesting that they remain associated with each other throughout serpentinization. The less strong correlation with Mo and Pd indicates complex geochemical interactions (Figure 8d,e). The positive correlation between Au with Co and Mn in millerite (Figure 8f,g) suggests that these elements may be incorporated during the oxidation of pentlandite, which occurs as serpentinization progresses. The oxidation process, likely driven by the transition from reducing to more oxidizing conditions, could facilitate the stability and co-precipitation of Au, Co, and Mn in millerite [61]. Violarite, a secondary sulfide, exhibits negative relationships between Au and elements such as Co and Mn (Figure 8h,i). Millerite and violarite are secondary minerals that typically form during the later stages of serpentinization, often under conditions that promote significant chemical re-equilibration [17,57]. These findings align with the hypothesis that serpentinization is a key process in the remobilization and recycling of Au within ultramafic environments, as it can create heterogeneous zones of Au enrichment [61,62].

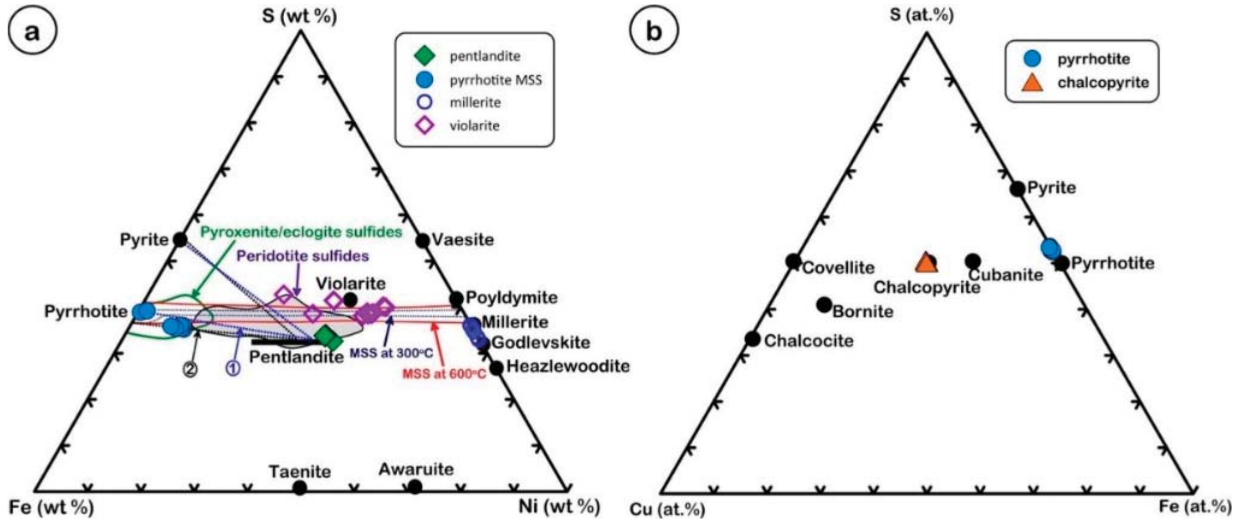

Figure 5. (**a**) Ternary (Fe-S-Ni) diagram showing electron probe microanalysis (EPMA) results for sulfides from the Abu Dahr area. Mineral end-members are taken from Craig [63], while compositional limits of mono-sulfide solid solution (MSS) at 300 °C and 600 °C are after Naldrett et al. [64]. Peridotite and pyroxenite sulfide fields are from Guo et al. [32] and Gréau et al. [65]. Tie-lines 1 and 2 correspond to the main interstitial sulfide assemblages of the Fe-Ni-S system after Lorand and Alard [66]. (**b**) Ternary (Cu-S-Fe) diagram showing EPMA results for chalcopyrite and pyrrhotite from the Abu Dahr area, black circles after Bortnikov et al. [67].

Table 3. LA-ICP-MS data of sulfide inclusions in serpentinized peridotites from the Gabal Abu Dahr ophiolite.

	LOD	**Pentlandite: n = 14**				**Nickeloan Pyrrhotite: n = 12**				**Chalcopyrite: n = 10**			
		Min	**Max**	**Average**	**STDV**	**Min**	**Max**	**Average**	**STDV**	**Min**	**Max**	**Average**	**STDV**
^{47}Ti	2.26	12.55	96.9	37.2	22.9	0.59	12.6	3.93	5.11				
^{51}V	0.18	5.94	156	25.2	38.1	0.03	1.9	0.48	0.68	1.12	3.85	2.77	1.45
^{52}Cr	2.08	15.02	1271	238	323								
^{55}Mn	1.11	57.8	662	353	196	0.02	55.9	14.43	19.9	6.45	28.31	13.95	9.8
^{59}Co	0.1	448	15,553	2855	3894	1113	4801	2715	1228	0.62	7.35	3.15	2.04
^{63}Cu	0.3	3.03	390	142	135	3.06	170	28.8	50.3				
^{66}Zn	0.36	1.66	26.5	7.28	7.43	1.67	41.16	6.9	11.89	468	1050	607	166
^{75}As	0.61	651	1053	836	112	3735	78,733	12,867	22,851				
^{77}Se	0.32	14.3	39.5	19.18	6.33								
^{95}Mo	0.11	0.68	33.2	3.49	8.57	0.11	2.34	0.7	0.87				
^{105}Pd	0.14	0.02	0.18	0.08	0.05	0.01	0.2	0.06	0.08	10.9	14.53	12.62	1.18
^{109}Ag	0.08	0.25	6.64	1.39	1.65	0	6.51	1.01	1.92	1.58	67.46	15.72	24.5
^{111}Cd	0.32	0.03	0.09	0.06	0.02	0	0.05	0.02	0.02	64.6	187	114	40.0
^{120}Sn	0.15	0.04	0.08	0.05	0.02					1.74	44.67	13.5	13.59
^{123}Sb	0.35	3.7	34.38	15.02	8.62	3.32	115.66	19.26	33.94	1.34	10.48	5.1	4.78
^{184}W	0.08	2.86	30.12	11.58	7.88	0	0.08	0.03	0.03				
^{193}Ir	0.05	0	0.01	0.01	0	0.02	0.34	0.09	0.12	0.12	0.35	0.23	0.17
^{195}Pt	0.26	0.02	0.26	0.08	0.08								
^{197}Au	0.05	0.17	6.11	1.99	1.83	0.03	0.41	0.11	0.12				
^{205}Tl	0.06	0.29	3.87	1.38	1								
^{208}Pb	0.13	9.68	26.1	18.4	5.3	10.55	361	60.1	106	1.14	86.2	23.52	25.23
^{209}Bi	0.07	0.55	2.41	1.24	0.47	0.02	0.80	0.13	0.24	0.26	14.32	3.55	4.33
^{60}Ni	0.05					3770	98,018	15,683	28,278	1.61	74.31	17.2	31.94
S/Se		8543	23,174	18,381	3779								

	Millerite: n = 8				Violarite: n = 11			
	Min	Max	Average	STDV	Min	Max	Average	STDV
	20.9	267	114	91.4	10.7	234	79.8	68.8
^{47}Ti	20.4	105	52.3	33.2	2.79	124	54.4	40.7
^{51}V	45.2	797	322	293	7.59	1973	300	635
^{52}Cr	380	2619	886	725	203	607	440	126
^{55}Mn	1492	13,776	8443	5397	25,354	42,679	33,623	5336
^{59}Co	66.6	1351	542	379	8.45	538	230	177
^{63}Cu	3.16	215	44.7	74.5	2.02	54.8	15.5	20.1
^{66}Zn	1082	3342	1870	755	939	2052	1294	325
^{75}As	37.44	75.1	50.19	12.96	2.52	81.69	24.3	24.0
^{77}Se	1.6	87.42	30.55	38.53	1.72	247	57.02	76.3
^{95}Mo	0.05	0.61	0.25	0.25				
^{105}Pd	0.23	18.29	5.73	6.24	0.34	2.3	1.23	0.58
^{109}Ag	0.07	0.83	0.4	0.39				
^{111}Cd	0.06	0.27	0.12	0.1				
^{120}Sn	11.2	50.8	25.6	13.5	5.47	80.8	26.2	20.8
^{123}Sb	5.87	47.5	19.8	14.8	2.82	120	34.2	33.0
^{184}W								
^{193}Ir	0.08	0.13	0.11	0.04				
^{195}Pt	0.06	0.32	0.19	0.13	0.09	0.12	0.11	0.02
^{197}Au	0.72	4.91	2.47	1.78	0.2	6.89	1.77	2.21
^{205}Tl	17.2	114	45.2	32.1	5.94	60.7	32.5	18.7
^{208}Pb	1.44	3.82	2.71	0.8	0.62	4.04	1.99	1
^{209}Bi								
^{60}Ni	4526	9177	7129	1667	4546	160,925	45,133	505,245

Blank cells = below detection or quantification limits.

The correlations between Au and various chalcophile elements like Ag, Se, Cu, and Bi in the studied sulfide minerals provide valuable insights into the geochemical behavior of Au during the serpentinization of ultramafic rocks. In pentlandite (Figure 9a,b), there is a positive correlation between Au and Ag, as well as between Au and Se. This suggests that during earlier magmatic processes, Au co-precipitated with Ag and Se, indicating that pentlandite might host these elements under specific conditions. The scatter in the data points, however, suggests that while pentlandite can accommodate Au, it does so inconsistently, likely involving trace amounts or micro-inclusions rather than significant lattice incorporation [59,68,69]. Nickeloan pyrrhotite, formed from MSS during serpentinization, shows a strong positive correlation is observed between Au and Cu, suggesting that Cu facilitates the incorporation of Au into pyrrhotite during the serpentinization process (Figure 9c–e). This is consistent with the behavior of Cu as a chalcophile element that often associates with Au in sulfide minerals. Additionally, the positive correlation between Au and Sb indicates that Sb also plays a role in stabilizing Au within pyrrhotite, possibly through substitution mechanisms within the mineral's structure. These correlations reflect the strong affinity of Au for these elements during the crystallization of pyrrhotite from monosulfide solid solution (MSS) [61]. The tight clustering of data along the trend lines suggests that Au, together with these chalcophile elements, is preferentially partitioned into nickeloan pyrrhotite during mineralization processes, reflecting their mutual compatibility within the sulfide lattice [70]. In millerite (Figure 9f,g), the data shows a negative correlation between Au and Bi, and a positive correlation between Au and Sb. The negative correlation with Bi suggests that as Bi content increases, Au concentration decreases, implying that Bi may not favor the incorporation of Au in millerite. Conversely, the positive correlation between Au and Sb indicates that Sb may play a more significant role in accommodating Au within millerite, possibly through substitution or co-precipitation during later stages of serpentinization. This suggests that millerite can serve as a host for Au, particularly in association with Sb, though it does so under specific geochemical conditions and less consistently than pyrrhotite [71]. Violarite shows weak with a slight positive correlation with Ag and a slight negative correlation with Cu (Figure 9h,i). This indicates that violarite does not serve as a primary host for Au. Instead, the weak and somewhat inverse relationships suggest that the presence of Au in violarite is likely due to remobilization during later stages of serpentinization or alteration rather than through primary mineralization processes. The role of violarite in hosting Au appears incidental, possibly capturing Au from surrounding minerals during late stage serpentinization or alteration events [53,72,73].

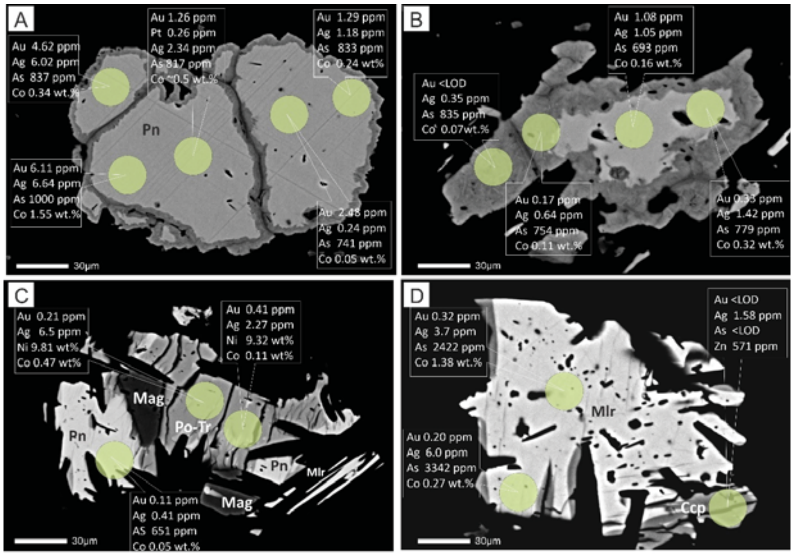

Figure 6. Backscattered electron (BSE) images of sulfide inclusions in serpentinized peridotites from the Gabal Abu Dahr ophiolite. The gradual transformation of pentlandite into violarite, with visibly

cracked boundaries demarcating the transition zones. Abbreviations: chalcopyrite (Ccp), magnetite (Mag), millerite (Mlr), pentlandite (Pn), pyrrhotite (Po), tremolite (Tr), and violarite (Vr). (**A**) Partially altered pentlandite in a carbonatized peridotite sample, (**B**) Extensively altered pentlandite replaced by violarite in a serpentinite sample, (**C**) Intergrowths of pentlandite, MSS and magnetite and millerite in a serpentinite sample (**D**) Millerite intergrown with chalcopyrite in a listvenite sample.

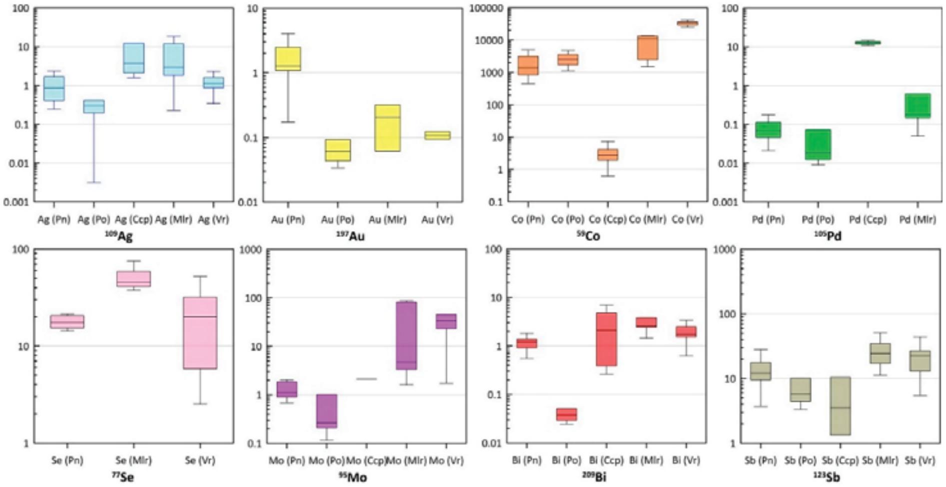

Figure 7. Box and whisker plots showcasing the LA-ICP-MS data, elucidating compositional discrepancies among the analyzed mineral phases. Abbreviations: chalcopyrite (Ccp); millerite (Mlr); pentlandite (Pn); pyrrhotite (Po); and violarite (Vr).

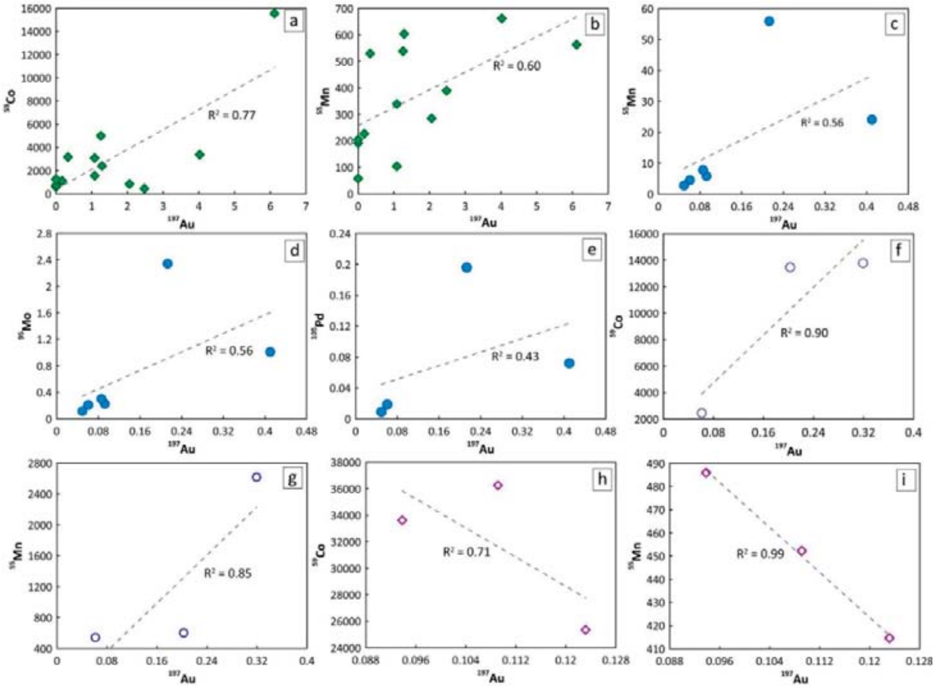

Figure 8. Correlation between ^{197}Au and a variety of siderophile elements, such as ^{195}Pt, ^{95}Mo, ^{55}Mn, ^{105}Pd, ^{193}Ir, and ^{59}Co, in the following minerals: (**a**,**b**) pentlandite, (**c**–**f**) pyrrhotite, (**g**) millerite, and (**h**,**i**) violarite.

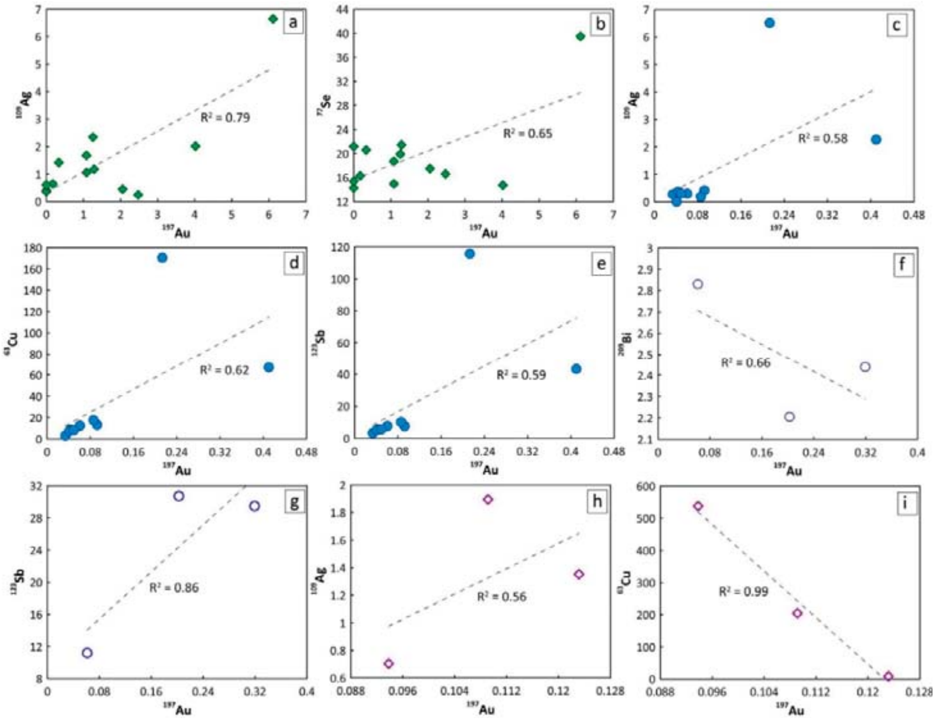

Figure 9. Correlation between ^{197}Au and a variety of chalcophile elements, such as ^{109}Ag, ^{77}Se, ^{63}Cu, ^{123}Sb, and ^{209}Bi in the following minerals: (**a**,**b**) pentlandite, (**c**–**e**) pyrrhotite, (**f**,**g**) millerite, and (**h**,**i**) violarite.

6. Discussion

6.1. The Significance of the S/Se Ratios in Ni-Sulfides

The S/Se ratios in Ni-sulfides unveil a multifaceted narrative of geochemical processes shaping their formation. The Earth's mantle emerges as a pivotal reservoir, furnishing sulfur for various geological phenomena. Studies by Eckstrand and Hulbert [74], McDonough and Sun [75], Hattori et al. [76], and Lorand et al. [77] consistently denote a relatively uniform S/Se ratio within the mantle, typically falling between 2850 and 4350. This unwavering range features the fundamental role of mantle-derived sulfur in the genesis of Ni-sulfides. In contrast, meteoritic materials show a lower S/Se ratio of 2500 ± 270 as stated by Dreibus et al. [78], which is likely due to sulfur depletion or selenium enrichment resulting from processes such as volatility during nebular condensation [79], fractional crystallization [80], and aqueous alteration on parent bodies [81]. Meanwhile, magmatic sulfides within Earth's crust exhibit a broad spectrum of S/Se ratios ranging from 4363 to 10,932 [82] and from 3500 to 100,000 according to Yamamoto [83], reflecting the intricate interplay of sulfur sources and geochemical processes within crustal environments.

The S/Se ratios serve as a key guiding the exploration of Ni-sulfide origins, elucidating the complex geochemical tapestry woven across different geological domains. The mantle's steadfast S/Se ratios underscore its significance as a primary sulfur source, orchestrating diverse geological phenomena. Conversely, meteoritic materials offer glimpses into early solar system geochemistry, characterized by distinct elemental ratios compared to Earth's mantle. Within the Earth's crust, magmatic sulfides exhibit a wide range of S/Se ratios, reflective of the intricate interplay between diverse sulfur sources and geochemical processes. Collectively, these insights underscore the nuanced interplay of geochemical factors shaping the genesis of Ni-sulfides and underscore the importance of understanding sulfur's journey through Earth's geological history.

The observed S/Se ratios in the pentlandite, millerite, and violarite samples (ave. 18,381, 7129, and 45,133, respectively) significantly exceed typical mantle values, indicating a substantial contribution of sulfur from crustal sources (Lorand et al., 2013). Beyond just the unusual S/Se ratios, there are additional signs pointing to the influence of subduction. The variation in S/Se ratios among these sulfide minerals is formed by several geological factors. For instance, the tectonic setting plays a crucial role. When sulfides form in a convergent margin, like a subduction zone, the S/Se ratios can differ compared to those formed in an intraplate setting [84,85]. Redox conditions also matter: oxidizing conditions generally favor sulfur incorporation into sulfides, while reducing conditions can lead to more selenium being incorporated [86,87]. Additionally, temperature and pressure during sulfide crystallization significantly affect the S/Se ratios. Higher temperatures promote selenium incorporation into minerals, whereas lower temperatures are more favorable for sulfur [88,89]. Moreover, post-magmatic processes like hydrothermal alteration can cause remobilization and redistribution of sulfur and selenium, which further modifies the original S/Se ratios [90]. Metamorphic processes, particularly those associated with pressure and temperature changes during regional metamorphism, can also lead to the breakdown and reformation of sulfide minerals, altering their S/Se ratios due to fluid interactions and mineralogical transformations [91,92]. Therefore, the observed fluctuations in S/Se ratios point towards a post-magmatic overprint, indicating further alteration subsequent to initial magmatic events. Moreover, the capability of Ni to be incorporated into the MSS at high temperatures, around 1000 °C [93], suggests a dynamic process where sulfur enrichment in MSS leads to subsequent recrystallization into minerals such as pentlandite and pyrrhotite at lower temperatures, typically ranging from 300 to 600 °C. As temperatures drop below 300 °C, the MSS undergoes dissolution, facilitating the formation of pyrite and pentlandite.

6.2. Implications of Pd Contents in the Examined Sulfides

Palladium is commonly associated with nickel sulfide minerals such as pentlandite and millerite, often occurring as trace elements or in solid solution within their crystal structures. Additionally, palladium can form distinct mineral phases, which are typically found in association with magmatic sulfides [94]. As the minerals undergo recrystallization at lower temperatures, Pd may remain incorporated within them, albeit potentially in variable concentrations depending on specific geochemical conditions. The dissolution of the MSS at temperatures below 300 °C and the formation of pyrite may influence the distribution of Pd in the sulfide mineral assemblage [94]. Palladium's affinity for sulfide minerals, coupled with temperature-dependent processes, could lead to varying concentrations and distributions of Pd in the different sulfide phases. The observed geochemical processes provide insights into the potential incorporation mechanisms and distribution patterns of Pd within sulfide minerals.

The evolution of sulfide liquids involves complex processes that influence the concentration and distribution of various elements, including those compatible or incompatible with MSS [94]. Elements like Co, Mo, Re, Rh, and IPGE (iridium-subgroup of the PGEs) tend to decrease in concentration as the sulfide liquid evolves, contrasting with whole rock compositions. Conversely, base-metal sulfides crystallizing from the evolving liquid exhibit higher concentrations of some incompatible elements such as Pd, Ag, Bi, Cd, In, Pb, Sn, Te, Tl, and Zn [94]. The distribution of Pd is influenced by mechanisms distinct from sulfide liquid fractionation, owing to its incompatibility with MSS and its association with the fractionated liquid [95,96]. Pentlandite formed solely through exsolution from MSS and intermediate solid solution tends to exhibit lower Pd concentrations, while pentlandite formed via peritectic reactions between MSS and fractionated sulfide liquid shows higher Pd concentrations [94].

Our data indicate that pentlandite contains a lower concentration of Pd, ≤ 0.18 ppm, suggesting that Pd is not incorporated into the pentlandite. This mineral forms through the exsolution of MSS and ISS with Ni-pyrrhotite, which exhibits Pd concentrations of ~ 0.2 ppm. Moreover, the characteristics of this pentlandite are consistent with those observed in pentlandite that crystallize from evolved Fe-rich MSS, as documented by Wei et al. [97], where Pd concentrations range from 0.1 to 0.5 ppm.

The incorporation of trace elements into the chalcopyrite structure is more challenging compared to other common BMS phases. This difficulty arises from the covalent bonding present in chalcopyrite, which prevents the application of Goldschmidt's rules typically used to predict partitioning trends in purely ionic structures [98,99]. The presence of trace elements in chalcopyrite is attributed to the co-crystallization of other sulfides in the same ore system, with Pd potentially exsolved from co-crystallizing base-metal sulfides during cooling or concentrated in fluid phases at shallow lithospheric levels, e.g., George et al. [98], Helmy et al. [100], and Mutschler et al. [101]. In the current study, the majority of the Pd in chalcopyrite (up to 14.53 ppm) was either attributed to the concentration of fluid phases at shallow intrusive levels [101] or exsolved from the co-crystallizing BMS during cooling [100].

6.3. Refertilization of the Lithospheric Mantle and Au Mobilization

Subduction zones, crucial for the recycling of materials between the Earth's surface and the mantle, contribute significantly to the formation of gold deposits. During subduction, fluids released from subducting slabs carry metals like Au into the overlying mantle wedge, enriching mantle rocks [102]. These metals can then be transported back to the surface through processes such as mantle melting and volcanic activity, leading to the formation of Au-bearing magmas and mineral deposits, e.g., Qiu et al. [103].

The presence of enriched source regions and/or melts is considered crucial for the formation of Au deposits [104–106]. Two prevailing hypotheses explain Au deposition: the subcontinental lithospheric mantle acting as the source of metal-rich magma, carrying Au as it migrates upwards through the overlaying crust, potentially via pathways from the underlying mantle, and enriched melts and fluids originating from mid- to lower crustal reservoirs, settling in the shallow layers of the crust [104,105,107]. Serpentinization of ultramafic rocks incorporates water into the rock matrix and can generate hydrogen and possibly hydrogen sulfide, which may contribute to the mobilization of metals, including Au [102]. Gold may be leached from mantle rocks during serpentinization and transported to shallower levels through the upward migration of fluids along fractures and faults [57].

In the Gabal Abu Dahr area, chromite in serpentinized peridotites has been found to originate from depleted mantle sources with a significant degree of partial melting in a sub-arc tectonic setting. These peridotite samples contain trace amounts of a BMS assemblage, including pentlandite, pyrrhotite, pyrite, and chalcopyrite, enveloped by secondary metamorphic sulfides like millerite and violarite. Pentlandite, considered a relic of mantle sulfide phases, is believed to have originated from sulfide melts trapped during partial melting events in the residual mantle [32,108,109]. Pyrrhotite forms when mafic magmas crystallize and become sulfur-saturated [110]. Chalcopyrite originates from the recrystallization of iron sulfide minerals from a copper-rich liquid at relatively low temperatures in shallow intrusive levels. During serpentinization, the extensive alteration of olivine and talc-carbonate significantly transforms the mineralogical and chemical environment, which destabilizes sulfur-bearing minerals such as pentlandite, leading to the extraction of sulfur and the subsequent formation of new sulfides and alloys through complex hydrothermal processes [111].

The higher Au content in pentlandite compared to violarite (Table 3) can be explained by the influence of peridotite-hosted hydrothermal systems in the Gabal Abu Dahr ophiolite, which exhibit a significant redox gradient during serpentinization [21,24–26,112]. The low Au content in violarite suggests precipitation from highly reduced fluids [113]. Violarite forms through the supergene oxidation of pentlandite at low temperatures, under acidic conditions with pH levels between 3 and 5 [72]. This process is considered a replacement reaction, as evidenced by the porous and fractured textures of the violarite grains, indicating a dissolution-reprecipitation event rather than a direct topotactic transformation, in line with observations by Putnis [114] and Pring et al. [73].

6.4. Geologic Evolution and Gold Recycling

The Gabal Abu Dahr ophiolites exhibit a complex geological history characterized by several transformative processes (Figure 9). Around 730 Ma, the area experienced subduction and the formation of a forearc basin. During this period, partial melting of a metasomatized mantle wedge, driven by the dehydration of the subducting slab, generated silicate melts. These melts played a significant role in the formation of subduction-related intrusions in the area [115] (Figure 10).

As subduction progressed, the mantle source became significantly depleted, leading to the formation of ultramafic residual rocks such as refractory peridotites [116]. These peridotites represent the residual mantle after extensive partial melting in a sub-arc tectonic setting and contribute to the formation of chromite and base-metal sulfide (BMS) assemblages. The presence of minerals such as pentlandite, pyrrhotite, pyrite, and chalcopyrite in these peridotites indicates the trapping of sulfide melts during the melting events. This process was critical in capturing and mobilizing Au within the mantle rocks in the region [117,118]. Additionally, the interaction between subducted slab fluids and the overlying mantle wedge led to extensive mantle metasomatism, which enriched the mantle with various elements, including Au (Figure 10).

Following subduction and partial melting, the section cooled, leading to the crystallization of mafic magma and the onset of sulfur saturation. This cooling allowed for the rare formation of immiscible sulfide melts, which incorporated base metals such as Ni, Co, and Au, trapping them within the mantle section as it cooled to about 1000 °C [59,119]. During the cooling phase, early sulfide assemblages in peridotites were enclosed by secondary sulfides: pentlandite formed from trapped sulfide melts, pyrrhotite from Ni-sulfide, and chalcopyrite from recrystallized Fe-sulfides in a Cu-rich liquid at lower temperatures [19,57] (Figure 10).

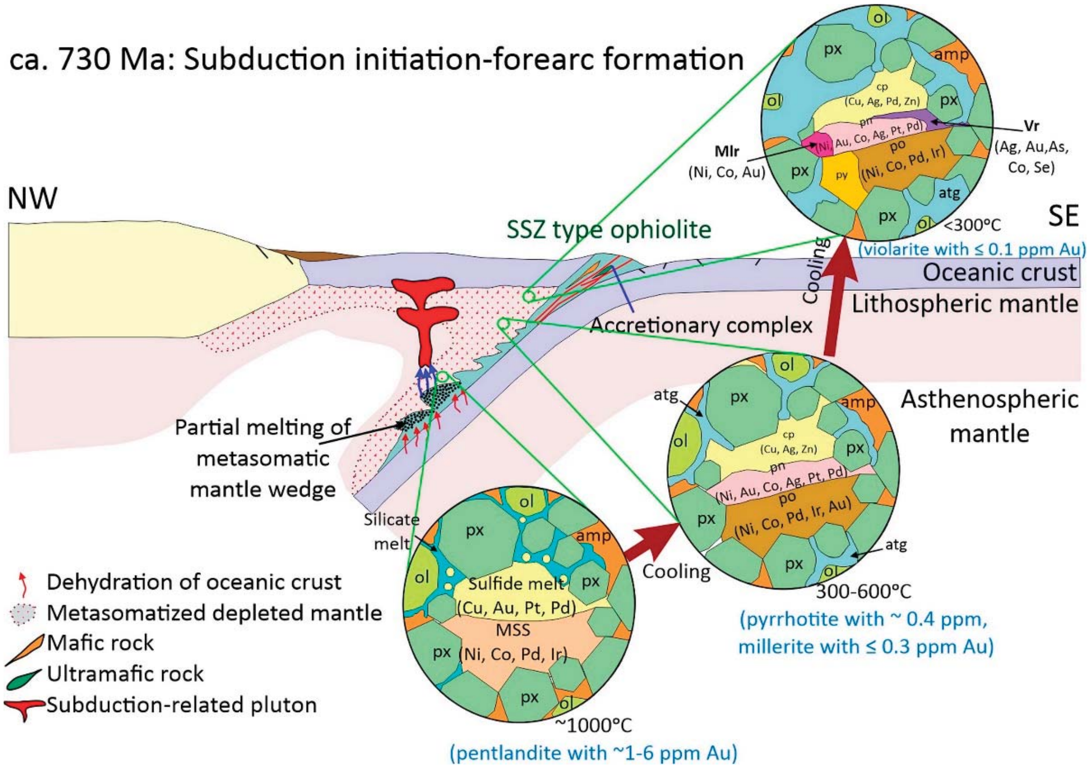

Figure 10. Conceptual model summarizing the evolution and gold recycling in the Gabal Abu Dahr ophiolites. To the west is a possibly old continental or island arc mass with mainly granitic composition.

The final stage involved serpentinization, where hydrothermal fluids interacted with peridotites in the forearc mantle at temperatures between 300 °C and 600 °C. This process caused the breakdown of primary minerals like olivine and sulfides, leading to the formation of serpentine minerals and the remobilization of sulfur. The elevated temperatures facilitated the formation of secondary metamorphic sulfides, such as millerite and violarite, from the breakdown of pentlandite and other primary sulfides. This alteration process was critical for the recycling of Au, as the newly formed sulfides could capture and concentrate Au from the surrounding rock matrix. The high-temperature conditions in the forearc mantle played a key role in the continuous mobilization and redistribution of Au within the lithospheric mantle [120,121] (Figure 10).

This model highlights the key roles of subduction, partial melting, cooling, and hydrothermal alteration. Supra-subduction zone-type peridotites, featuring minerals like clinopyroxene, amphibole, and plagioclase formed through the cooling and crystallization of sub-arc mantle melts. The development of an accretionary complex and forearc basin, resulting from the accumulation of sediments and altered oceanic crust at the overriding plate's leading edge, further contributes to the area's geological complexity (Figure 10).

7. Conclusions

The study of the Gabal Abu Dahr ophiolite provides significant insights into the geochemical evolution and metal mobilization processes in supra-subduction zone (SSZ) settings. Bulk rock geochemical data, along with electron microprobe and laser ablation ICP-MS analyses integrated with petrographic and SEM studies, highlight the crucial role of serpentinization and hydrothermal processes in redistributing Au and other HSEs within metasomatized peridotites. The observed distribution of Au among different sulfide minerals, such as pentlandite, pyrrhotite, millerite, and violarite, underscores the complex interplay between magmatic and hydrothermal processes influenced by fluctuating redox conditions and the composition of hydrothermal fluids.

Pentlandite, as the primary host of Au, retains higher concentrations due to its early magmatic formation and favorable crystallization conditions for Au incorporation. In contrast, secondary sulfides formed during progressive serpentinization, including millerite and violarite, display lower Au concentrations, reflecting selective mobilization and retention driven by oxidation and desulfurization reactions. The presence of calcite ± magnesite ± serpentine veins and mineral assemblages, such as acicular antigorite, magnetite, and goethite, further supports the influence of hydrothermal fluids in controlling metal mobility and the geochemical evolution of the ophiolitic rocks under varying fO_2 and fCO_2 conditions. These processes are consistent with geochemical studies, such as those by Leblanc [80], who investigated the remobilization of Au in ophiolitic complexes, and Lorand and Alard [122], who emphasized the role of sulfur in controlling the behavior of chalcophile elements, including Au, during the serpentinization of mantle peridotites.

Thermodynamic modeling, validated by the observed mineral assemblages and redox conditions in the Abu Dahr ophiolites, emphasizes the significance of oxidation-reduction reactions in the redistribution and concentration of Au and HSEs. This study illustrates the importance of serpentinization and hydrothermal alteration in SSZ ophiolites, highlighting their role in the metallogenesis of Au and other siderophile elements within the Earth's crust. It also offers a conceptual framework for understanding metal flux and geochemical processes in forearc ophiolitic environments, contributing to the broader understanding of mineralization in these geological settings.

Author Contributions: Conceptualization, B.Z. and A.H.; methodology, B.Z., A.A. and A.D.; validation, B.Z., A.H. and F.D.; formal analysis, A.A., A.D. and A.R.; investigation, B.Z., A.A. and A.D.; resources, A.H.; data curation, A.A. and A.D.; writing—original draft preparation, B.Z., A.A. and A.D.; writing—review and editing, B.Z., A.A. and A.H.; visualization, A.A., F.D. and A.R.; supervision, A.H. and B.Z.; project administration, A.H.; funding acquisition, A.H., B.Z. and A.A. All authors have read and agreed to the published version of the manuscript.

Funding: This research was funded by [German Research Foundation (DFG)] grant number (457324982) And The APC was waived for Basem Zoheir.

Data Availability Statement: Data are contained within the article.

Acknowledgments: The handling editor and two anonymous reviewers are thanked for their insightful comments and valuable suggestions, which greatly improved the earlier version of this manuscript. We gratefully acknowledge the support of the German Research Foundation (DFG) for supporting this research (Project No. 457324982). Additionally, Amr Abdelnasser expresses his gratitude to Istanbul Technical University for its support through the Scientific Research Project (BAP project ID: 45396, code: FHD-2024-45396).

Conflicts of Interest: The authors declare no conflict of interest.

References

1. Mungall, J.E. Roasting the mantle: Slab melting and the genesis of major Au and Au-rich Cu deposits. *Geology* **2002**, *30*, 915–918. [CrossRef]
2. Griffin, W.; O'Reilly, S.Y.; Afonso, J.C.; Begg, G. The composition and evolution of lithospheric mantle: A re-evaluation and its tectonic implications. *J. Petrol.* **2009**, *50*, 1185–1204. [CrossRef]
3. Luguet, A.; Reisberg, L. Highly siderophile element and ^{187}Os signatures in non-cratonic basalt-hosted peridotite xenoliths: Unravelling the origin and evolution of the post-Archean lithospheric mantle. *Rev. Mineral. Geochem.* **2016**, *81*, 305–367. [CrossRef]
4. Hamlyn, P.R.; Keays, R.R. Sulfur saturation and second-stage melts; application to the Bushveld platinum metal deposits. *Econ. Geol.* **1986**, *81*, 1431–1445. [CrossRef]
5. Boyle, R. *The Geochemistry of Gold and Its Deposits: Bulletin 280*; Geological Survey of Canada: Ottawa, ON, Canada, 1979; pp. 1–584.
6. Barnes, S.-J.; Maier, W.D. The fractionation of Ni, Cu and the noble metals in silicate and sulphide liquids. *Short Course Notes-Geol. Assoc. Can.* **1999**, *13*, 69–106.
7. Barnes, S.-J.; Naldrett, A.J. Fractionation of the platinum-group elements and gold in some komatiites of the Abitibi greenstone belt, northern Ontario. *Econ. Geol.* **1987**, *82*, 165–183. [CrossRef]
8. Palme, H.; O'Neill, H.S.C. Mantle Composition. In *Treatise on Geochemistry*; Carlson, R.W., Ed.; Elsevier-Pergamon: Oxford, UK, 2005; Volume 2, pp. 1–38.
9. Mitchell, R.H.; Keays, R.R. Abundance and distribution of gold, palladium and iridium in some spinel and garnet lherzolites: Implications for the nature and origin of precious metal-rich intergranular components in the upper mantle. *Geochim. Cosmochim. Acta* **1981**, *45*, 2425–2442. [CrossRef]
10. Large, R.R.; Maslennikov, V.V.; Robert, F.O.; Danyushevsky, L.V.; Chang, Z. Multistage Sedimentary and Metamorphic Origin of Pyrite and Gold in the Giant Sukhoi Log Deposit, Lena Gold Province, Russia. *Econ. Geol.* **2007**, *102*, 1233–1267. [CrossRef]
11. Morey, A.A.; Tomkins, A.G.; Bierlein, F.P.; Weinberg, R.F.; Davidson, G.J. Bimodal distribution of gold in pyrite and arsenopyrite: Examples from the Archean Boorara and Bardoc shear systems, Yilgarn craton, Western Australia. *Econ. Geol.* **2008**, *103*, 599–614. [CrossRef]
12. Cook, N.J.; Ciobanu, C.L.; Pring, A.; Skinner, W.; Shimizu, M.; Danyushevsky, L.; Saini-Eidukat, B.; Melcher, F. Trace and minor elements in sphalerite: A LA-ICPMS study. *Geochim. Cosmochim. Acta* **2009**, *73*, 4761–4791. [CrossRef]
13. Cook, N.J.; Ciobanu, C.L.; Meria, D.; Silcock, D.; Wade, B. Arsenopyrite-pyrite association in an orogenic gold ore: Tracing mineralization history from textures and trace elements. *Econ. Geol.* **2013**, *108*, 1273–1283. [CrossRef]
14. Pearce, J.A.; Lippard, S.; Roberts, S. Characteristics and tectonic significance of supra-subduction zone ophiolites. *Geol. Soc. Lond. Spec. Publ.* **1984**, *16*, 77–94. [CrossRef]
15. Boudier, F.; Nicolas, A. Harzburgite and lherzolite subtypes in ophiolitic and oceanic environments. *Earth Planet. Sci. Lett.* **1985**, *76*, 84–92. [CrossRef]
16. Lorand, J. Mineralogy and chemistry of Cu-Fe-Ni sulfides in orogenic-type spinel peridotite bodies from Ariege (Northeastern Pyrenees, France). *Contrib. Mineral. Petrol.* **1989**, *103*, 335–345. [CrossRef]
17. Frost, B.R. On the stability of sulfides, oxides, and native metals in serpentinite. *J. Petrol.* **1985**, *26*, 31–63. [CrossRef]
18. Klein, F.; Bach, W. Fe–Ni–Co–O–S phase relations in peridotite–seawater interactions. *J. Petrol.* **2009**, *50*, 37–59. [CrossRef]
19. Frost, B.R.; Beard, J.S. On silica activity and serpentinization. *J. Petrol.* **2007**, *48*, 1351–1368. [CrossRef]
20. Bach, W.; Paulick, H.; Garrido, C.J.; Ildefonse, B.; Meurer, W.P.; Humphris, S.E. Unraveling the sequence of serpentinization reactions: Petrography, mineral chemistry, and petrophysics of serpentinites from MAR 15 N (ODP Leg 209, Site 1274). *Geophys. Res. Lett.* **2006**, *33*, 4–7. [CrossRef]
21. Alt, J.C.; Shanks, W.C., III. Sulfur in serpentinized oceanic peridotites: Serpentinization processes and microbial sulfate reduction. *J. Geophys. Res. Solid Earth* **1998**, *103*, 9917–9929. [CrossRef]
22. Klein, F.; Bach, W.; McCollom, T.M. Compositional controls on hydrogen generation during serpentinization of ultramafic rocks. *Lithos* **2013**, *178*, 55–69. [CrossRef]

23. Eckstrand, O. The Dumont serpentinite; a model for control of nickeliferous opaque mineral assemblages by alteration reactions in ultramafic rocks. *Econ. Geol.* **1975**, *70*, 183–201. [CrossRef]
24. Delacour, A.; Früh-Green, G.L.; Bernasconi, S.M. Sulfur mineralogy and geochemistry of serpentinites and gabbros of the Atlantis Massif (IODP Site U1309). *Geochim. Cosmochim. Acta* **2008**, *72*, 5111–5127. [CrossRef]
25. Schwarzenbach, E.M.; Früh-Green, G.L.; Bernasconi, S.M.; Alt, J.C.; Shanks, W.C., III; Gaggero, L.; Crispini, L. Sulfur geochemistry of peridotite-hosted hydrothermal systems: Comparing the Ligurian ophiolites with oceanic serpentinites. *Geochim. Cosmochim. Acta* **2012**, *91*, 283–305. [CrossRef]
26. Schwarzenbach, E.M.; Gazel, E.; Caddick, M.J. Hydrothermal processes in partially serpentinized peridotites from Costa Rica: Evidence from native copper and complex sulfide assemblages. *Contrib. Mineral. Petrol.* **2014**, *168*, 1079. [CrossRef]
27. Abrajano, T.A.; Pasteris, J.D. Zambales ophiolite, Philippines. *Contrib. Mineral. Petrol.* **1989**, *103*, 64–77. [CrossRef]
28. Tsushima, N.; Matsueda, H.; Ishihara, S. Polymetallic mineralization at the Nakakoshi copper deposits, central Hokkaido, Japan. *Resour. Geol.* **1999**, *49*, 89–97. [CrossRef]
29. Zappettini, E.; Picot, P.; Sabourdy, G. Nouvelles données sur le gisement aurifère du Châtelet (Massif Central français), liaison génétique probable entre l'or et les roches ultrabasiques. *C.-R. Séances L'académie Sci. Série 2 Mécanique-Phys. Chim. Sci. L'univers Sci. Terre* **1983**, *297*, 351–354.
30. Buisson, G.; Leblanc, M. Gold in mantle peridotites from Upper Proterozoic ophiolites in Arabia, Mali, and Morocco. *Econ. Geol.* **1987**, *82*, 2091–2097. [CrossRef]
31. Vaughan, D.J.; Corkhill, C.L. Mineralogy of sulfides. *Elements* **2017**, *13*, 81–87. [CrossRef]
32. Guo, J.; Griffin, W.L.; O'Reilly, S.Y. Geochemistry and Origin of Sulphide Minerals in Mantle Xenoliths: Qilin, Southeastern China. *J. Petrol.* **1999**, *40*, 1125–1149. [CrossRef]
33. Alard, O.; Griffin, W.L.; Lorand, J.P.; Jackson, S.E.; O'Reilly, S.Y. Non-chondritic distribution of the highly siderophile elements in mantle sulphides. *Nature* **2000**, *407*, 891–894. [CrossRef] [PubMed]
34. Griffin, W.; Graham, S.; O'Reilly, S.Y.; Pearson, N. Lithosphere evolution beneath the Kaapvaal Craton: Re–Os systematics of sulfides in mantle-derived peridotites. *Chem. Geol.* **2004**, *208*, 89–118. [CrossRef]
35. Kiseeva, E.S.; Fonseca, R.O.; Smythe, D.J. Chalcophile elements and sulfides in the upper mantle. *Elements* **2017**, *13*, 111–116. [CrossRef]
36. Andronikov, A.V.; Andronikova, I.E.; Sidorinova, T. Trace-Element Geochemistry of Sulfides in Upper Mantle Lherzolite Xenoliths from East Antarctica. *Minerals* **2021**, *11*, 773. [CrossRef]
37. Fontboté, L.; Kouzmanov, K.; Chiaradia, M.; Pokrovski, G.S. Sulfide minerals in hydrothermal deposits. *Elements* **2017**, *13*, 97–103. [CrossRef]
38. Ashmawy, M.H. *The Ophiolitic Mélange of the South Eastern Desert of Egypt: Remote Sensing, Field Work and Petrographic Investigations*; D. Reimer: Winnipeg, MB, Canada, 1987; Volume 84.
39. Zoheir, B.A.; Mehanna, A.M.; Qaoud, N.N. Geochemistry and geothermobarometry of the Um Eleiga Neoproterozoic island arc intrusive complex, SE Egypt: Genesis of a potential gold-hosting intrusion. *Appl. Earth Sci.* **2008**, *117*, 89–111. [CrossRef]
40. Gahlan, H.A.; Azer, M.K.; Khalil, A.E. The neoproterozoic Abu Dahr ophiolite, South Eastern Desert, Egypt: Petrological characteristics and tectonomagmatic evolution. *Mineral. Petrol.* **2015**, *109*, 611–630. [CrossRef]
41. Seleem, T.; Hamimi, Z.; Zaky, K.; Zoheir, B.A. ASTER mapping and geochemical analysis of chromitite bodies in the Abu Dahr ophiolites, South Eastern Desert, Egypt. *Arab. J. Geosci.* **2020**, *13*, 731. [CrossRef]
42. Zoheir, B.; Abd El-Rahman, Y.; Kusky, T.; Xiong, F. New SIMS zircon U-Pb ages and oxygen isotope data for ophiolite nappes in the Eastern Desert of Egypt: Implications for Gondwana assembly. *Gondwana Res.* **2022**, *105*, 450–467. [CrossRef]
43. Longerich, H.P.; Jackson, S.E.; Günther, D. Inter-laboratory note. Laser ablation inductively coupled plasma mass spectrometric transient signal data acquisition and analyte concentration calculation. *J. Anal. At. Spectrom.* **1996**, *11*, 899–904. [CrossRef]
44. Garbe-Schönberg, D.; Müller, S. Nano-particulate pressed powder tablets for LA-ICP-MS. *J. Anal. At. Spectrom.* **2014**, *29*, 990–1000. [CrossRef]
45. El-Bayoumi, R. Ophiolites and melange complex of Wadi Ghadir area, Eastern Desert, Egypt. *Precambrian Res.* **1982**, *16*, A17–A18. [CrossRef]
46. Basta, F.F.; Maurice, A.E.; Bakhit, B.R.; Ali, K.A.; Manton, W.I. Neoproterozoic contaminated MORB of Wadi Ghadir ophiolite, NE Africa: Geochemical and Nd and Sr isotopic constraints. *J. Afr. Earth Sci.* **2011**, *59*, 227–242. [CrossRef]
47. Azer, M.K.; Gahlan, H.A.; Asimow, P.D.; Mubarak, H.S.; Al-Kahtany, K.M. Multiple stages of carbonation and element redistribution during formation of ultramafic-hosted magnesite in Neoproterozoic ophiolites of the Arabian-Nubian Shield, Egypt. *J. Geol.* **2019**, *127*, 81–107. [CrossRef]
48. Evans, B.W.; Hattori, K.; Baronnet, A. Serpentinite: What, why, where? *Elements* **2013**, *9*, 99–106. [CrossRef]
49. Xie, Z.; Hattori, K.; Dong, Y.; Wang, J. In situ characterization of forearc serpentinized peridotite from the Sulu ultrahigh-pressure terrane: Behavior of fluid-mobile elements in continental subduction zone. *Geosci. Front.* **2021**, *12*, 101139. [CrossRef]
50. Boskabadi, A.; Pitcairn, I.K.; Leybourne, M.I.; Teagle, D.A.H.; Cooper, M.J.; Hadizadeh, H.; Nasiri Bezenjani, R.; Monazzami Bagherzadeh, R. Carbonation of ophiolitic ultramafic rocks: Listvenite formation in the Late Cretaceous ophiolites of eastern Iran. *Lithos* **2020**, *352–353*, 105307. [CrossRef]
51. Gahlan, H.A.; Azer, M.K.; Asimow, P.D.; Al-Kahtany, K.M. Petrogenesis of gold-bearing listvenites from the carbonatized mantle section of the Neoproterozoic Ess ophiolite, Western Arabian Shield, Saudi Arabia. *Lithos* **2020**, *372–373*, 105679. [CrossRef]

52. Akbulut, M.; Pïşkïn, Ö.; Karayïğït, A.İ. The genesis of the carbonatized and silicified ultramafics known as listvenites: A case study from the Mihalıççık region (Eskişehir), NW Turkey. *Geol. J.* **2006**, *41*, 557–580. [CrossRef]
53. Imai, N.; Mariko, T.; Shiga, Y. Supergene alteration of pentlandite to violarite Contribution ot the knowledge of secondary violarite. *Min. Geol.* **1978**, *28*, 1–11.
54. Lorand, J.-P.; Luguet, A. Chalcophile and siderophile elements in mantle rocks: Trace elements controlled by trace minerals. *Rev. Mineral. Geochem.* **2016**, *81*, 441–488. [CrossRef]
55. Rüpke, L.H.; Morgan, J.P.; Hort, M.; Connolly, J.A.D. Serpentine and the subduction zone water cycle. *Earth Planet. Sci. Lett.* **2004**, *223*, 17–34. [CrossRef]
56. Groves, D.I.; Goldfarb, R.J.; Gebre-Mariam, M.; Hagemann, S.; Robert, F. Orogenic gold deposits: A proposed classification in the context of their crustal distribution and relationship to other gold deposit types. *Ore Geol. Rev.* **1998**, *13*, 7–27. [CrossRef]
57. Deschamps, F.; Godard, M.; Guillot, S.; Hattori, K. Geochemistry of subduction zone serpentinites: A review. *Lithos* **2013**, *178*, 96–127. [CrossRef]
58. Malvoisin, B. Mass transfer in the oceanic lithosphere: Serpentinization is not isochemical. *Earth Planet. Sci. Lett.* **2015**, *430*, 75–85. [CrossRef]
59. Naldrett, A.J. *Magmatic Sulfide Deposits: Geology, Geochemistry and Exploration*; Springer: Berlin/Heidelberg, Germany, 2004; pp. XVIII, 728.
60. Brenan, J.M.; Andrews, D. High-temperature stability of laurite and Ru–Os–Ir alloy and their role in PGE fractionation in mafic magmas. *Can. Mineral.* **2001**, *39*, 341–360. [CrossRef]
61. Hattori, K.H.; Guillot, S. Geochemical character of serpentinites associated with high-to ultrahigh-pressure metamorphic rocks in the Alps, Cuba, and the Himalayas: Recycling of elements in subduction zones. *Geochem. Geophys. Geosyst.* **2007**. [CrossRef]
62. Augé, T. Chromite deposits in the northern Oman ophiolite: Mineralogical constraints. *Miner. Depos.* **1987**, *22*, 1–10. [CrossRef]
63. Craig, J.R. Pyrite-pentlandite assemblages and other low temperature relations in the Fe-Ni-S system. *Am. J. Sci.* **1973**, *273*, 496–510.
64. Naldrett, A.; Craig, J.; Kullerud, G. The central portion of the Fe-Ni-S system and its bearing on pentlandite exsolution in iron-nickel sulfide ores. *Econ. Geol.* **1967**, *62*, 826–847. [CrossRef]
65. Gréau, Y.; Alard, O.; Griffin, W.L.; Huang, J.-X.; O'Reilly, S.Y. Sulfides and chalcophile elements in Roberts Victor eclogites: Unravelling a sulfide-rich metasomatic event. *Chem. Geol.* **2013**, *354*, 73–92. [CrossRef]
66. Lorand, J.-P.; Alard, O. Pyrite tracks assimilation of crustal sulfur in Pyrenean peridotites. *Mineral. Petrol.* **2011**, *101*, 115–128. [CrossRef]
67. Bortnikov, N.; Vikentyev, I.; Apollonov, V.; Stavrova, O.; Bogdanov, Y.; Lein, A.; Gurvich, E.; Sagalevich, A.; Simonov, V.; Ikorskii, S. The Rainbow serpentinite-related hydrothermal field, Mid-Atlantic Ridge, 36 14rN: Mineralogical and geochemical features. In Proceedings of the Joint Sixth Meeting. Mineral Deposits at the Beginning of the 21st Century, Krakow, Poland, 26–29 August 2001; pp. 265–268.
68. Simon, A.C.; Pettke, T.; Candela, P.A.; Piccoli, P.M.; Heinrich, C.A. Magnetite solubility and iron transport in magmatic-hydrothermal environments. *Geochim. Cosmochim. Acta* **2004**, *68*, 4905–4914. [CrossRef]
69. Tomkins, A.G. Windows of metamorphic sulfur liberation in the crust: Implications for gold deposit genesis. *Geochim. Cosmochim. Acta* **2010**, *74*, 3246–3259. [CrossRef]
70. Melekestseva, I.; Maslennikov, V.; Tret'yakov, G.; Maslennikova, S.; Danyushevsky, L.; Kotlyarov, V.; Large, R.; Beltenev, V.; Khvorov, P. Trace element geochemistry of sulfides from the Ashadze-2 hydrothermal field (12°58′ N, Mid-Atlantic Ridge): Influence of host rocks, formation conditions or seawater? *Minerals* **2020**, *10*, 743. [CrossRef]
71. Wang, Y.; Gao, J.; Huang, X.; Qi, L.; Lyu, C. Trace element composition of magnetite from the Xinqiao Fe–S (–Cu–Au) deposit, Tongling, Eastern China: Constraints on fluid evolution and ore genesis. *Acta Geochim.* **2018**, *37*, 639–654. [CrossRef]
72. Tenailleau, C.; Pring, A.; Etschmann, B.; Brugger, J.; Grguric, B.; Putnis, A. Transformation of pentlandite to violarite under mild hydrothermal conditions. *Am. Mineral.* **2006**, *91*, 706–709. [CrossRef]
73. Pring, A.; Tenailleau, C.; Etschmann, B.; Brugger, J.; Grguric, B. The transformation of pentlandite to violarite under mild hydrothermal conditions: A dissolution-reprecipitation reaction. In *Regolith 2005: Ten Years of CRC LEME. Proceedings of the CRC LEME Regional Regolith Symposia 2005*; CRC LEME: Bentley, WA, USA, 2005; pp. 252–255. Available online: https://citeseerx.ist.psu.edu/document?repid=rep1&type=pdf&doi=36c66679065e58a541fadf4953266dce47ea2b32 (accessed on 3 September 2024).
74. Eckstrand, O.; Hulbert, L. Selenium and the source of sulfur in magmatic nickel and platinum deposits [abs.]. *Geological Association of Canada-Mineralogical Association Canada Program with Abstracts*. 1987, p. 40. Available online: https://scholar.google.com/scholar_lookup?title=Selenium%20and%20the%20source%20of%20sulfur%20in%20magmatic%20nickel%20and%20platinum%20deposits%20:%20Geological%20Association%20of%20CanadaMineralogical%20Association%20Canada%20Program%20with%20Abstracts&publication_year=1987&author=O.R.%20Eckstrand&author=L.J.%20Hulbert (accessed on 4 September 2024).
75. McDonough, W.F.; Sun, S.-S. The composition of the Earth. *Chem. Geol.* **1995**, *120*, 223–253. [CrossRef]
76. Hattori, K.H.; Arai, S.; Clarke, D.B. Selenium, tellurium, arsenic and antimony contents of primary mantle sulfides. *Can. Mineral.* **2002**, *40*, 637–650. [CrossRef]
77. Lorand, J.-P.; Alard, O.; Luguet, A.; Keays, R.R. Sulfur and selenium systematics of the subcontinental lithospheric mantle: Inferences from the Massif Central xenolith suite (France). *Geochim. Cosmochim. Acta* **2003**, *67*, 4137–4151. [CrossRef]

78. Dreibus, G.; Palme, H.; Spettel, B.; Zipfel, J.; Wänke, H. Sulfur and selenium in chondritic meteorites. *Meteoritics* **1995**, *30*, 439–445. [CrossRef]
79. Lodders, K. Solar system abundances and condensation temperatures of the elements. *Astrophys. J.* **2003**, *591*, 1220. [CrossRef]
80. Leblanc, M. Platinum-Group Elements and Gold in Ophiolitic Complexes: Distribution and Fractionation from Mantle to Oceanic Floor. In *Ophiolite Genesis and Evolution of the Oceanic Lithosphere: Proceedings of the Ophiolite Conference, Muscat, Oman, 7–18 January 1990*; Springer: Dordrecht, The Netherlands, 1991; pp. 231–260.
81. Hellmann, J.L.; Hopp, T.; Burkhardt, C.; Kleine, T. Origin of volatile element depletion among carbonaceous chondrites. *Earth Planet. Sci. Lett.* **2020**, *549*, 116508. [CrossRef]
82. Holwell, D.A.; Fiorentini, M.L.; Knott, T.R.; McDonald, I.; Blanks, D.E.; Campbell McCuaig, T.; Gorczyk, W. Mobilisation of deep crustal sulfide melts as a first order control on upper lithospheric metallogeny. *Nat. Commun.* **2022**, *13*, 573. [CrossRef]
83. Yamamoto, M. Relationship between Se/S and sulfur isotope ratios of hydrothermal sulfide minerals. *Miner. Depos.* **1976**, *11*, 197–209. [CrossRef]
84. Savov, I.P.; Ryan, J.G.; D'Antonio, M.; Kelley, K.; Mattie, P. Geochemistry of serpentinized peridotites from the Mariana Forearc Conical Seamount, ODP Leg 125: Implications for the elemental recycling at subduction zones. *Geochem. Geophys. Geosyst.* **2005**. [CrossRef]
85. Rapp, R.P.; Watson, E.B.; Miller, C.F. Partial melting of amphibolite/eclogite and the origin of Archean trondhjemites and tonalites. *Precambrian Res.* **1991**, *51*, 1–25. [CrossRef]
86. Fleet, M.E. XANES spectroscopy of sulfur in earth materials. *Can. Mineral.* **2005**, *43*, 1811. [CrossRef]
87. Hanley, J.; Mungall, J.; Spooner, E.; Pettke, T. Fluid and melt inclusion evidence for platinum-group element transport by high salinity fluids and halide melts below the JM Reef, Stillwater Complex. In Proceedings of the Montana, USA: 10th International Platinum Symposium "Platinum-Group Elements-from Genesis to Beneficiation and Environmental Impact", Oulu, Finland, 8–11 August 2005; pp. 94–97.
88. Mungall, J.E.; Brenan, J.M. Partitioning of platinum-group elements and Au between sulfide liquid and basalt and the origins of mantle-crust fractionation of the chalcophile elements. *Geochim. Cosmochim. Acta* **2014**, *125*, 265–289. [CrossRef]
89. O'Neil, H.S.C.; Mavrogenes, J.A. The sulfide capacity and the sulfur content at sulfide saturation of silicate melts at 1400 °C and 1 bar. *J. Petrol.* **2002**, *43*, 1049–1087. [CrossRef]
90. Blanks, D.E.; Holwell, D.A.; Barnes, S.J.; Schoneveld, L.E.; Fiorentini, M.L.; Baublys, K.A.; Mbiri, L.; Knott, T.R. Mobilization and Fractionation of Magmatic Sulfide: Emplacement and Deformation of the Munali Ni-(Cu-Platinum Group Element) Deposit, Zambia. *Econ. Geol.* **2022**, *117*, 1709–1729. [CrossRef]
91. Sharp, Z.D.; Essene, E.J.; Kelly, W.C. A re-examination of the arsenopyrite geothermometer: Pressure considerations and applications to natural assemblages. *J. Mineral. Assoc. Can.* **1985**, *23*, 517–534.
92. Evans, K.; Powell, R.; Frost, B. Using equilibrium thermodynamics in the study of metasomatic alteration, illustrated by an application to serpentinites. *Lithos* **2013**, *168*, 67–84. [CrossRef]
93. Holwell, B.D.; McDonald, I. A review of the behaviour of platinum group elements within natural magmatic sulfide ore systems. *Platin. Met. Rev.* **2010**, *54*, 26–36. [CrossRef]
94. Mansur, E.T.; Barnes, S.-J.; Duran, C.J. Textural and compositional evidence for the formation of pentlandite via peritectic reaction: Implications for the distribution of highly siderophile elements. *Geology* **2019**, *47*, 351–354. [CrossRef]
95. Barnes, S.-J.; Cox, R.A.; Zientek, M.L. Platinum-group element, gold, silver and base metal distribution in compositionally zoned sulfide droplets from the Medvezky Creek Mine, Noril'sk, Russia. *Contrib. Mineral. Petrol.* **2006**, *152*, 187–200. [CrossRef]
96. Dare, S.; Barnes, S. The origin of Pd in pentlandites from Creighton mine, Ni-Cu-PGE deposit, Sudbury, Canada. In *Xi'an International Platinum Symposium, 174*; Ontario Geological Survey, Miscellaneous Release–Data 269: Sudbury Ontario, ON, Canada, 2009.
97. Wei, B.; Yan Wang, C.; Dong, Y. Behavior of palladium during fractionation of sulfide liquid: New constraints from the Kalatongke Cu-Ni sulfide-bearing intrusion in the central Asian orogenic belt, NW China. *Ore Geol. Rev.* **2023**, *160*, 105578. [CrossRef]
98. George, L.L.; Cook, N.J.; Ciobanu, C.L. Partitioning of trace elements in co-crystallized sphalerite–galena–chalcopyrite hydrothermal ores. *Ore Geol. Rev.* **2016**, *77*, 97–116. [CrossRef]
99. Goldschmidt, V. *Geochemistry*; Clarendon: Oxford, UK, 1954; Volume 624, pp. 1–730.
100. Helmy, H.M.; Ballhaus, C.; Berndt, J.; Bockrath, C.; Wohlgemuth-Ueberwasser, C. Formation of Pt, Pd and Ni tellurides: Experiments in sulfide–telluride systems. *Contrib. Mineral. Petrol.* **2007**, *153*, 577–591. [CrossRef]
101. Mutschler, F.; Griffin, M.; Stevens, D.; Shannon, S., Jr. Precious metal deposits related to alkaline rocks in the North American Cordillera—An interpretive review: Transactions Geological Society of South Africa. *South Afr. J. Geol.* **1985**, *88*, 355–377.
102. Mitchell, A.L.; Grove, T.L. Experiments on melt–rock reaction in the shallow mantle wedge. *Contrib. Mineral. Petrol.* **2016**, *171*, 1–21. [CrossRef]
103. Qiu, K.-F.; Deng, J.; Laflamme, C.; Long, Z.-Y.; Wan, R.-Q.; Moynier, F.; Yu, H.-C.; Zhang, J.-Y.; Ding, Z.-J.; Goldfarb, R. Giant Mesozoic gold ores derived from subducted oceanic slab and overlying sediments. *Geochim. Cosmochim. Acta* **2023**, *343*, 133–141. [CrossRef]
104. Sillitoe, R.H. Special paper: Major gold deposits and belts of the North and South American Cordillera: Distribution, tectonomagmatic settings, and metallogenic considerations. *Econ. Geol.* **2008**, *103*, 663–687. [CrossRef]

105. Begg, G.C.; Hronsky, J.A.; Arndt, N.T.; Griffin, W.L.; O'Reilly, S.Y.; Hayward, N. Lithospheric, cratonic, and geodynamic setting of Ni-Cu-PGE sulfide deposits. *Econ. Geol.* **2010**, *105*, 1057–1070. [CrossRef]
106. Webber, A.; Roberts, S.; Taylor, R.; Pitcairn, I.K. Golden plumes: Substantial gold enrichment of oceanic crust during ridge-plume interaction. *Geology* **2013**, *41*, 87–90. [CrossRef]
107. Core, D.P.; Kesler, S.E.; Essene, E.J. Unusually Cu-rich magmas associated with giant porphyry copper deposits: Evidence from Bingham, Utah. *Geology* **2006**, *34*, 41–44. [CrossRef]
108. Dromgoole, E.L.; Pasteris, J.D. Interpretation of the sulfide assemblages in a suite of xenoliths. *Mantle Metasomatism Alkaline Magmat.* **1987**, *215*, 25.
109. Szabó, C.; Bodnar, R. Chemistry and origin of mantle sulfides in spinel peridotite xenoliths from alkaline basaltic lavas, Nógraád-Gömör Volcanic Field, northern Hungary and southern Slovakia. *Geochim. Cosmochim. Acta* **1995**, *59*, 3917–3927. [CrossRef]
110. Andersen, T.; Griffin, W.; O'Reilly, S.Y. Primary sulphide melt inclusions in mantle-derived megacrysts and pyroxenites. *Lithos* **1987**, *20*, 279–294. [CrossRef]
111. Barnes, S.J.; Wells, M.A.; Verrall, M.R. Effects of magmatic processes, serpentinization, and talc-carbonate alteration on sulfide mineralogy and ore textures in the Black Swan disseminated nickel sulfide deposit, Yilgarn Craton. *Econ. Geol.* **2009**, *104*, 539–562. [CrossRef]
112. Delacour, A.; Früh-Green, G.L.; Bernasconi, S.M.; Kelley, D.S. Sulfur in peridotites and gabbros at Lost City (30 N, MAR): Implications for hydrothermal alteration and microbial activity during serpentinization. *Geochim. Cosmochim. Acta* **2008**, *72*, 5090–5110. [CrossRef]
113. Oberthuer, T.; Mumm, A.; Vetter, U.; Simon, K.; Amanor, J. Gold mineralization in the Ashanti Belt of Ghana; genetic constraints of the stable isotope geochemistry. *Econ. Geol.* **1996**, *91*, 289–301. [CrossRef]
114. Putnis, A. Mineral replacement reactions: From macroscopic observations to microscopic mechanisms. *Mineral. Mag.* **2002**, *66*, 689–708. [CrossRef]
115. Peacock, S.M. Fluid processes in subduction zones. *Science* **1990**, *248*, 329–337. [CrossRef]
116. Pearce, J.A. Supra-subduction zone ophiolites: The search for modern analogues. *Spec. Pap.-Geol. Soc. Am.* **2003**, *373*, 269–293.
117. Bebout, G.E. Volatile transfer and recycling at convergent margins: Mass-balance and insights from high-P/T metamorphic rocks. *Subduction Top Bottom* **1996**, *96*, 179–193.
118. Kerrich, R.; Goldfarb, R.; Groves, D.; Garwin, S. *The Geodynamics of World-Class Gold Deposits: Characteristics, Space-Time Distribution, and Origins; Reviews in Economic Geology*; GeoScienceWorld: McLean, VA, USA, 2000; Volume 13, pp. 501–551.
119. Barnes, S.-J.; Lightfoot, P.C. *Formation of Magmatic Nickel Sulfide Deposits and Processes Affecting Their Copper and Platinum Group Element Contents*; GeoScienceWorld: McLean, VA, USA, 2005. [CrossRef]
120. Andreani, M.; Muñoz, M.; Marcaillou, C.; Delacour, A. μXANES study of iron redox state in serpentine during oceanic serpentinization. *Lithos* **2013**, *178*, 70–83. [CrossRef]
121. Garuti, G.; Pushkarev, E.V.; Zaccarini, F.; Cabella, R.; Anikina, E. Chromite composition and platinum-group mineral assemblage in the Uktus Uralian-Alaskan-type complex (Central Urals, Russia). *Miner. Depos.* **2003**, *38*, 312–326. [CrossRef]
122. Lorand, J.-P.; Alard, O. Platinum-group element abundances in the upper mantle: New constraints from in situ and whole-rock analyses of Massif Central xenoliths (France). *Geochim. Cosmochim. Acta* **2001**, *65*, 2789–2806. [CrossRef]

Disclaimer/Publisher's Note: The statements, opinions and data contained in all publications are solely those of the individual author(s) and contributor(s) and not of MDPI and/or the editor(s). MDPI and/or the editor(s) disclaim responsibility for any injury to people or property resulting from any ideas, methods, instructions or products referred to in the content.